Key Points:

- Calculation and comparison of carbonate accumulation rates depend on solid age models
- Geographic and paleobathymetric carbonate accumulation rates were highly variable during the middle and late Eocene
- Surface carbonate production and ocean ventilation were important drivers of the middle and late Eocene carbonate accumulation rates

Middle to Late Eocene Changes of the Ocean Carbonate Cycle

C. Borrelli[1] [iD]**, M. E. Katz[2], and J. R. Toggweiler[3]** [iD]

[1]Department of Earth and Environmental Sciences, University of Rochester, Rochester, NY, USA, [2]Department of Earth and Environmental Sciences, Rensselaer Polytechnic Institute, Troy, NY, USA, [3]Geophysical Fluid Dynamics Laboratory, NOAA, Princeton, NJ, USA

Abstract Sedimentary records show that calcium carbonate ($CaCO_3$) preservation fluctuated during the Eocene. These fluctuations are well documented for the equatorial Pacific. However, data from other basins are sparse. In this study, we report new middle and late Eocene bulk calcium carbonate percentages and accumulation rates from the northwestern Pacific (Ocean Drilling Program—ODP—Site 884) and the Atlantic (ODP Sites 1053, 1090, and 1263) Oceans; in addition, we calculate $CaCO_3$ accumulation rates for sites with published percentage bulk $CaCO_3$ to expand geographic and paleobathymetric coverage. Using these data, we investigate the response of the carbonate cycle to environmental changes (e.g., temperatures, primary productivity, weathering, and ocean circulation) at the beginning of the greenhouse-icehouse transition (∼43–34 Ma). Our results show that in the middle to late Eocene $CaCO_3$ accumulation rates were highly variable at different paleodepths and ocean basins suggesting that the evolution of carbonate accumulation rates over the Eocene was influenced by different processes in different locations. In particular, our data emphasize the role of surface $CaCO_3$ production and ocean ventilation in driving changes in $CaCO_3$ preservation and burial at the seafloor. Our study also highlights the need for a better understanding of the processes regulating $CaCO_3$ surface production today in order to correctly interpret geological records.

Plain Language Summary Over geological timescales, $CaCO_3$ production in the ocean surface and burial in marine sediments are important components of the global carbon cycle. A rapid increase in $CaCO_3$ preservation at deeper depths occurred at the Eocene/Oligocene boundary. However, what drove this change is still debated. Here, we investigate $CaCO_3$ accumulation at sites from different paleodepths and ocean basins during the middle and late Eocene (∼43–34 Ma). This is a particularly important period of time as it marks the beginning of the greenhouse-to-icehouse climate transition. Our results show that $CaCO_3$ accumulation and dissolution were spatially and temporally heterogeneous. Based on this, we propose that $CaCO_3$ production at the ocean surface, as well as changes in ocean circulation, had a fundamental role in driving $CaCO_3$ preservation in different ocean basins.

1. Introduction

The carbonate cycle includes three processes: (a) calcium carbonate ($CaCO_3$) production at the surface; (b) sinking of $CaCO_3$ particles through the water column, where these particles are susceptible to dissolution; and (b) settling and burial of $CaCO_3$ particles in sediments (Broecker & Peng, 1982; Sarmiento & Gruber, 2006).

We refer to surface $CaCO_3$ productivity as the carbonate production due to calcification in the euphotic layer (or surface ocean) (e.g., Berelson et al., 2007). This production is still not very well constrained and this lack of knowledge influences the interpretation of geological records. Coccolithophores are considered the biggest contributors to $CaCO_3$ surface production (Sarmiento & Gruber, 2006), even if it has been proposed that foraminifera and pteropods might be important contributors, as well (e.g., Iglesias-Rodriguez et al., 2002). Coccolithophores can be found in eutrophic environments at temperate and high latitudes; however, most species live in oligotrophic, warm waters (e.g., Brand, 1994; Rost & Riebesell, 2004). This preference is reflected in the $CaCO_3$ content of modern sediments (see, for example, Figure 1d in Dunne et al., 2012).

Traditionally, $CaCO_3$-rich sediments are expected above the lysocline and $CaCO_3$-free sediments are expected below the calcium carbonate compensation depth (CCD) (e.g., Boudreau et al., 2018; Broecker & Peng, 1982; Ridgwell & Zeebe, 2005; Sarmiento & Gruber, 2006; Zeebe & Wolf-Gladrow, 2001). However, modern observations show that a significant amount of $CaCO_3$ (40%–80%; Milliman et al., 1999) dissolves at depths much shallower than the top of the lysocline (e.g., Balch & Kilpatrick, 1996; Martin & Sayles, 1996; Milliman et al., 1999)

highlighting that the traditional conceptual model of $CaCO_3$ preservation driven by marine chemistry (i.e., the lysocline and the CCD) may no longer be a satisfactory explanation of the $CaCO_3$ distribution today and in the geological record.

On time scales of hundreds of thousands of years and longer, $CaCO_3$ production and dissolution are fundamental components of the global carbon cycle because these processes affect ocean alkalinity, the dissolved inorganic carbon (DIC) pool, and indirectly the CO_2 concentration in the atmosphere (Sarmiento & Gruber, 2006; Zeebe, 2012). The link between the $CaCO_3$ cycle and the CO_2 concentration in the atmosphere can be summarized with the concept of "$CaCO_3$ compensation," or the ability of the ocean carbonate system to react to alkalinity imbalances via variations in $CaCO_3$ preservation and dissolution at the seafloor (Broecker & Peng, 1987). Alkalinity imbalances are mainly caused by changes in the weathering of calcium carbonate and calcium silicate rocks driven by variations in atmospheric CO_2 concentrations and surface temperatures (e.g., Berner & Caldeira, 1997; Ridgwell & Zeebe, 2005; Walker et al., 1981). Although the weathering of carbonate rocks and consequent $CaCO_3$ burial does not affect the Earth's surface CO_2 budget (due to the stoichiometry of the carbonate weathering reaction), the weathering of silicates leading to $CaCO_3$ production at the ocean surface and burial in deep sediments represents a net loss of CO_2 stored in the surface ocean and atmosphere (e.g., Berner, 1999; Ridgwell & Zeebe, 2005). This is an important negative feedback, which is thought to control atmospheric CO_2 concentration over geological time scales (e.g., Berner & Caldeira, 1997; Broecker & Sanyal, 1998; Walker et al., 1981). Eventually, carbon locked in sediment is recycled back to the atmosphere, mainly via decarbonation after subduction of sediments (e.g., Berner, 1999; Ridgwell & Zeebe, 2005).

The middle Eocene-early Oligocene (40-33 Ma) was a time of global change. Earth shifted to a climate characterized by lower atmospheric CO_2, colder temperatures, build-up of permanent ice sheets on Antarctica, and possibly episodic Northern Hemisphere glaciations (e.g., Anagnostou et al., 2016, 2020; Aubry & Bord, 2009; Cramer et al., 2011; Cramwinckel et al., 2018; DeConto & Pollard, 2003; Foster et al., 2017; Katz et al., 2008; Lear et al., 2008; Liu et al., 2009; Miller et al., 2008; Pagani et al., 2011; Thomas, 2007; Tripati & Darby, 2018; Wade & Pearson, 2008; Wade et al., 2012; Zachos et al., 1994, 2001). In addition, key oceanic gateways opened (e.g., Abelson et al., 2008; Allen & Armstrong, 2008; Clift et al., 1995; Livermore et al., 2007; Stickley et al., 2004) and ocean circulation changed (e.g., Abelson & Erez, 2017; Borrelli et al., 2014; Borrelli & Katz, 2015; Coxall et al., 2018; Cramer et al., 2009; Katz et al., 2011; Langton et al., 2016; Scher & Martin, 2006). Finally, a key element of this global change is thought to be the increased preservation of $CaCO_3$ at deeper depths ∼33.9 Ma (the "deepening of the CCD;" e.g., Coxall et al., 2005; Pälike et al., 2012; Rea & Lyle, 2005; Tripati et al., 2005; Van Andel, 1975). However the mechanisms responsible for this change are still debated.

The study of the east equatorial Pacific sedimentary records, and in particular of the ODP Site 1218 matching high-resolution carbonate accumulation rates (CARs) and benthic foraminiferal $\delta^{18}O$ and $\delta^{13}C$, demonstrated a synchronicity between the increase of $CaCO_3$ accumulation at deeper depths and ice sheet build-up in Antarctica (Coxall et al., 2005). In this context, it was proposed that a deeper CCD was triggered by a shift in $CaCO_3$ deposition from shallow to deeper waters (shelf-basin fractionation) and an increase in old limestone erosion that delivered more dissolved inorganic carbon and alkalinity to the oceans (Coxall et al., 2005), as supported by modeling simulations (Merico et al., 2008). However, several studies proposed alternative scenarios. For example, Miller et al. (2009) argued that a more vigorous thermohaline circulation with shorter deep-water residence time affected $CaCO_3$ burial at deeper depths. Rea and Lyle (2005) hypothesized that increased Ca delivery from the continents to the oceans was the main driver of the change in sediment composition. Similarly, Basak and Martin (2013) proposed that $CaCO_3$ preservation was facilitated by an increase in ocean alkalinity influenced by weathering of Antarctic carbonate basement rocks. Finally, a modeling study (Armstrong McKay et al., 2016) identified a reduction in carbonate burial in shelf environments, an increase in shelf carbonate weathering, and sequestration of organic matter in permafrost and peatlands as the main processes responsible for the Eocene/Oligocene (E/O) boundary carbonate sedimentary records (i.e., CCD deepening and benthic $\delta^{13}C$ excursion).

Analysis of middle and late Eocene sedimentary records showed that the increased $CaCO_3$ preservation at deeper depths starting at the E/O boundary was preceded by episodes of high CARs, called carbonate accumulation events (CAEs) (CAEs 1–7) (Lyle et al., 2005; Pälike et al., 2012; Tripati et al., 2005). These episodes are well constrained for the equatorial Pacific, but sparse data sets are available from other locations (Pälike et al., 2012; Peterson & Backman, 1990; Thunell & Corliss, 1986; Tripati et al., 2005). Considering the duration and amplitude of the equatorial Pacific CAEs, Earth-system model simulations identified variations in the type (labile vs.
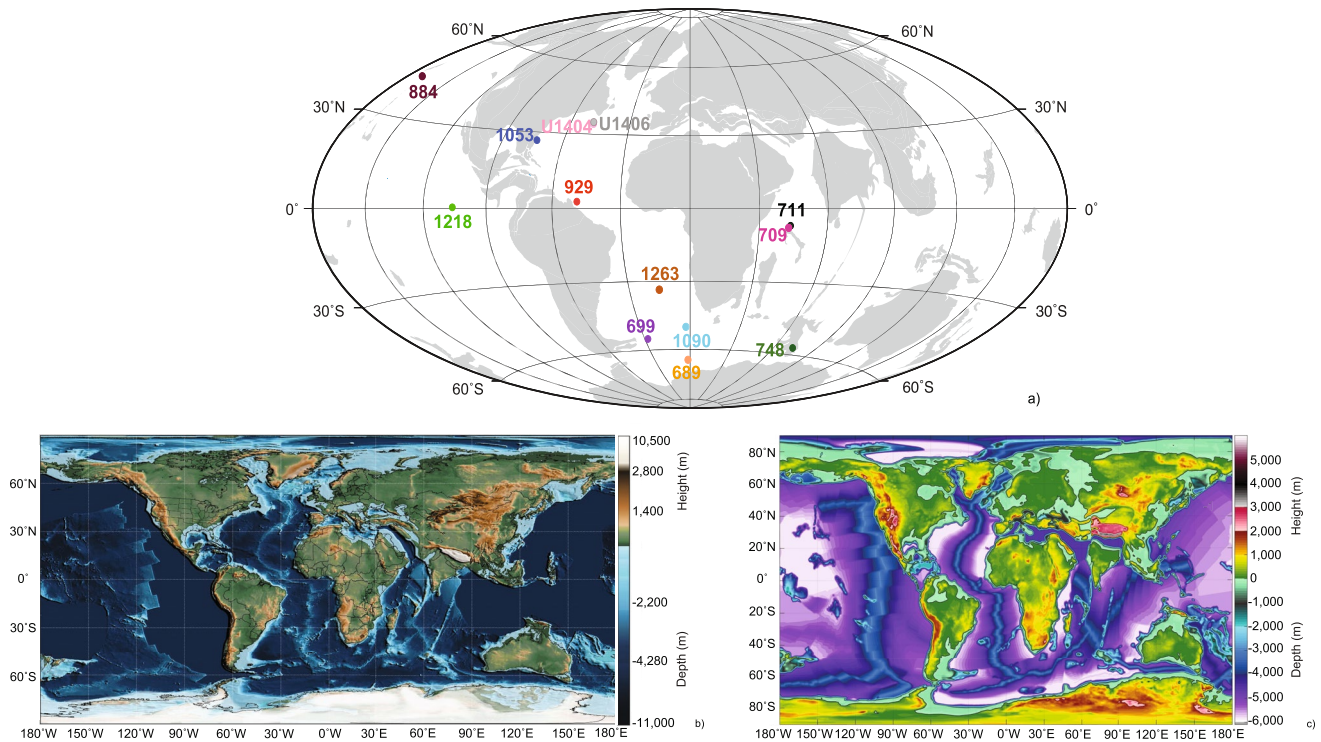
Figure 1. Late Eocene (38 Ma) maps. (a) Approximate paleolocation of the sites used in this study. The base map was generated from http://www.odsn.de. (b) Paleogeographic reconstruction (40 Ma) by Scotese (2021). Reproduced with permission. (c) Paleogeographic reconstruction (38 Ma) by Baatsen et al. (2016). Reproduced with permission. Following the approach of Hutchison et al. (2021), (b and c) are shown to highlight the uncertainties in middle to late Eocene paleogeography. See Hutchison et al. (2021) for a discussion on the topic.

refractory) and amount of organic carbon in sediments, possibly coupled to changes in weathering rates, as the mechanism responsible for the equatorial Pacific sedimentary records (Pälike et al., 2012). Specifically, an initial low amount of labile organic carbon would promote $CaCO_3$ accumulation in sediments because of less $CaCO_3$ dissolution in the water column. This mechanism would be of particular importance in regions characterized by high surface primary productivity, such as the eastern equatorial Pacific (Pälike et al., 2012). However, we note that in Pälike et al. (2012), changes in ocean circulation and residence times could not be evaluated due to the absence of records from the North Atlantic.

In this study, we constrain changes in $CaCO_3$ production and burial during the middle-late Eocene (~43–34 Ma). We build a global data set of carbonate accumulation rates (mass of preserved $CaCO_3$ per unit of seafloor area per unit of time). In particular, we analyzed middle to late Eocene samples from the northwestern Pacific (Ocean Drilling Program, ODP, Site 884) and the Atlantic (ODP Sites 1053, 1263, and 1090) Oceans. We emphasize that the investigation of carbonate records from the North Pacific and Atlantic (vs. equatorial Pacific; e.g., Pälike et al., 2012) is novel and of paramount importance as these regions have been proposed as sites of deep water formation during the middle and late Eocene (Baatsen, von der Heydt, Huber, et al., 2018; Baatsen, von der Heydt, Kliphuis, et al., 2018; Borrelli & Katz, 2015; Borrelli et al., 2014; Hutchison et al., 2018; McKinley et al., 2019), in addition to the Southern Ocean (e.g., Pak and Miller, 1995; Thomas, 2004; Via & Thomas, 2006). We also calculated CARs for additional published data sets from other ODP and IODP (Integrated Ocean Drilling Program) locations in the Pacific, Atlantic, Indian, and Southern Oceans (Figure 1; Table 1) to expand geographic and paleobathymetric coverage.

Utilizing carbonate accumulation rates is a well-established method to study $CaCO_3$ burial (e.g., Coxall et al., 2005; Lyle et al., 2005; Pälike et al., 2012). Compared to the more traditional sediment $CaCO_3$ weight percent, which is not linear with $CaCO_3$ flux at the seafloor, CARs are standardized to sediment bulk density and are not influenced by dissolution of less-resistant sedimentary components (e.g., biogenic opal) or dilution by more resistant non-$CaCO_3$ material (e.g., clay) (Broecker & Peng, 1982; Lyle, 2003; Lyle et al., 2005).

Table 1
Summary of the Sites Used in This Study

Site	Location	Coordinates	Paleodepth (m)	References
ODP Site 884B	Northwestern Pacific Ocean (Detroit Seamount)	51°27.026'N, 168°20.228'E	~3,000–3,300	Borrelli and Katz (2015)[a]; Pak and Miller (1995); Shipboard Scientific Party (1993)[b]; this study
ODP Site 1053A	Northwestern Atlantic Ocean (Blake Nose)	29°59.5385′N, 76°31.4135′W	~1,500–1,750	Borrelli et al. (2014)[a]; Katz et al. (2011); Shipboard Scientific Party (1998)[b]; this study
ODP Site 1090B	Sub-Antarctic Atlantic Ocean (Agulhas Ridge)	42°54.821'S, 8°53.984'E	~3,000–3,300	Pusz et al. (2011); Shipboard Scientific Party (1999a, 1999b[b]); this study[a]
ODP Site 1263B	Southeastern Atlantic Ocean (Walvis Ridge)	28°31.960'S, 2°46.765'E	~1,900–2,100	Bohaty et al. (2009); Shipboard Scientific Party (2004a, 2004b[b]); Westerhold et al. (2020)[a]; this study
ODP Site 689B	Southern Ocean (Maud Rise)	64°31.009'S, 03°05.996'E	~1,500–1,800	Bohaty and Zachos (2003)[a]; Shipboard Scientific Party (1988a)[b]
ODP Site 699A	Sub-Antarctic Atlantic Ocean (East Georgia Basin)	51°32.537'S, 30°40.619'W	~3,400	Langton et al. (2016)[a]; Mead et al. (1993)[a]; Shipboard Scientific Party (1988b)[b]
ODP Site 709C	Equatorial Indian Ocean (Madingley Rise)	03°54.9'S, 60°33.1'E	~2,100–2,500	Bohaty et al. (2009); Peterson and Backman (1990)[a]; Shipboard Scientific Party (1988c)[b]
ODP Site 711A	Equatorial Indian Ocean (Madingley Rise)	02°44.56'S, 61°09.78'E	~3,400–3,700	Bohaty et al. (2009); Peterson and Backman (1990)[a]; Shipboard Scientific Party (1988d)[b]
ODP Site 748B	Sub-Antarctic Indian Ocean (Kerguelen Plateau)	58°26.45'S, 78°58.89'E	~700–900	Bohaty et al. (2009); Bohaty and Zachos (2003)[a]; Shipboard Scientific Party (1989)[b]
ODP Site 929E	Western equatorial Atlantic Ocean (Ceara Rise)	5°58.568'N, 43°44.402'W	~3,900	Kordesch et al. (2015); Pagani et al. (2011)[a]; Shipboard Scientific Party (1995)[b]
ODP Site 1218	Equatorial Pacific Ocean	08°53.38'N, 135°22.00'W	~2,900–3,900	Lyle et al. (2005); Pälike et al. (2012); Shipboard Scientific Party (2002)
IODP Site U1404A	Northwestern Atlantic Ocean (J-Anomaly Ridge)	40°00.7997′N, 51°48.5990′W	~4,000–4,200	Norris et al. (2014a[a,b], 2014c)
IODP Site U1406A	Northwestern Atlantic Ocean (J-Anomaly Ridge)	40°20.9992′N, 51°38.9994′W	~3,000–3,200	Norris et al. (2014b[a,b], 2014c)

[a]Source of the site-specific age model. Age models are reported in Tables S1–S13 in Supporting Information S1. Sample sedimentation rates (m/Ma) are reported in Figure S1 in Supporting Information S1. [b]Bulk (gamma ray attenuation, wet, and dry) density data and, when needed, $CaCO_3$ weight percent data, were retrieved from: https://www.ngdc.noaa.gov/mgg/curator/data/joides_resolution; and http://iodp.tamu.edu/janusweb/links/links_all.shtml.
Note. ODP = Ocean Drilling Program; IODP = Integrated Ocean Drilling Program.

We cover a paleodepth range between 700 and 4,000 m. If we assume that the ocean hypsometry in the middle and late Eocene was similar to the modern one (see Figure 1 in Pälike et al., 2012; cf. Rea & Lyle, 2005), our data sets represent ~35% of the ocean floor allowing us to test the hypothesis that in the middle and late Eocene (~43–34 Ma) carbonate burial was geographically and bathymetrically heterogeneous. Testing this hypothesis should yield insight on the influence that regional changes (enhancement in $CaCO_3$ surface productivity; an increase in bottom water ventilation) and global changes (cooling; weathering) had on carbonate preservation at the seafloor at the beginning of the greenhouse-to-icehouse climate transition. We focus on CAR changes over Myr time scales because the lower temporal resolution of several sedimentary records do not provide the basis for interpreting the data on higher-resolution time scales (10 to hundred thousand years).

2. Materials and Methods

We analyzed bulk sediment carbonate content from middle Eocene to lower Oligocene sections of ODP Sites 884 Hole B (Cores 74–83), 1053 Hole A (Cores 1–20), 1090 Hole B (Cores 35–41), and 1263 Hole B (Cores 4–8). Site 884 was drilled on the flank of the Detroit Seamount in the northwestern Pacific (51°27.026′N, 168°20.228′E; present depth 3,825 m; Figure 1) (Shipboard Scientific Party, 1993). Site 884 paleodepth was estimated to be ~3,000–3,300 m during the time period investigated (Pak & Miller, 1995). Site 1053 was cored on the upper part of the Blake Nose in the northwestern Atlantic (29°59.5385′N, 76°31.4135′W; present depth 1,630 m; Figure 1)

(Shipboard Scientific Party, 1998). In the Eocene, the Site 1053 paleodepth was estimated to be 1,500–1,700 m (Katz et al., 2011). Site 1090 was drilled on the southern flank of Agulhas Ridge in the Sub-Antarctic South Atlantic (42°54.821′S, 08°53.984′E; present depth 3,700 m; Figure 1) (Shipboard Scientific Party, 1999a, 1999b). The Site 1090 paleodepth was placed at ∼3,000–3,300 around 34 Ma (Pusz et al., 2011). Site 1263 was cored at Walvis Ridge in the southeastern Atlantic (28°31.960′S, 2°46.765′E; present depth 2,717 m; Figure 1) (Shipboard Scientific Party, 2004a, 2004b). The Site 1263 paleodepth was estimated at ∼1,900–2,100 m in the middle Eocene-early Oligocene (Bohaty et al., 2009).

The data collected for this study were compared with other ODP and IODP (Integrated Ocean Drilling Program) data sets (Sites 689, 699, 709, 711, 748, 929, 1218, U1404, and U1406; Figure 1; Table 1) to gain a comprehensive understanding of the variations of the oceanic $CaCO_3$ cycle during the middle and late Eocene (43–34 Ma).

2.1. Age Models

Carbonate accumulation rates are heavily dependent on the age models used and the time scale chosen. For this study, we used published age models (explained more in detail below), with the exception of Site 1090, for which a new age model was necessary (no published middle to early late Eocene age models were available). Sample ages are reported according to the 2012 Geological Time Scale (Gradstein et al., 2012). Westerhold et al. (2014) demonstrated how the sedimentation rates at various sites located in the equatorial Pacific can vary when different time scales are used for the age model (cfr. Figure S11 in Westerhold et al., 2014). We evaluate changes in sedimentation rates at our sites when different time scales are used by comparing the sedimentation rates according to the 2012 Geological Time Scale and the time scale of the original age model for each site (Figure S1 in Supporting Information S1). This comparison revealed that the sedimentation rates were relatively comparable among different time scales.

For Sites 689, 699, 748, 884, 929, 1053, and 1263, sample ages were calculated using published age models (Bohaty & Zachos, 2003; Borrelli et al., 2014; Borrelli & Katz, 2015; Langton et al., 2016; Mead et al., 1993; Pagani et al., 2011; Westerhold et al., 2020). A new age model was developed for Site 1090 as part of this study (Table S1 in Supporting Information S1) and it was based on magnetostratigraphic and calcareous nannoplankton datums (Channell et al., 2003; Marino & Flores, 2002). For Sites U1404 and U1406, sample ages were calculated according to the datum tie points published in the Expedition 342 sites reports (Norris et al., 2014a, 2014b). The sample ages for Sites 709 and 711 were available (Peterson & Backman, 1990). Because in Pälike et al. (2012) the ages of the Site 1218 samples were reported according to the Expedition 320 Time Scale (Pälike et al., 2010; Westerhold et al., 2012), we recalculated the sample ages according to the 2012 Geological Time Scale using the age model of Pälike et al. (2012) (Pälike et al., 2012; Westerhold et al., 2012). All age model are reported in Tables S1–S13 in Supporting Information S1.

For Sites 689, 699, 709, 711, 748, 884, 929, and 1053 sample ages were converted from the time scale of the respective published age models to the 2012 Geological Time Scale using the Ocean Drilling Stratigraphic Network (ODSN) time scale converter tool available online (http://www.odsn.de/odsn/services/conv_ts/conv_ts.html). This tool converts ages from one time scale to another using magnetic events.

For the Site 1263 sample ages, we could not use the ODSN converter tool, as there is no option available to convert the ages as published in Westerhold et al. (2020) to the 2012 Geological Time Scale. Because of this, we converted the Westerhold et al. (2020) age model (Table S11 in Supporting Information S1) to the 2012 Geological Time Scale using the paleomagnetic reversal ages.

The age model tie points for Sites U1404, and U1406 were available according to the 2012 Geological Time Scale, so no age conversion was necessary for these sites.

2.2. Sediment Carbonate Content Analysis and Calculation of Carbonate Accumulation Rates

Bulk sediment samples from Sites 884, 1053, 1090, and 1263 were analyzed for $CaCO_3$ weight percent. Measurements were conducted using an UIC Inc. CM5012 CO_2 Coulometer with an Automate FX Inc. automated sample acidification and delivery carousel, at the Lamont-Doherty Earth Observatory of Columbia University (New York, NY). Approximately 4–12 grams of homogenized dried sediment were used for analysis. Samples were acidified with 10% phosphoric acid and ultra-high-purity nitrogen gas was used as the carrier gas. The machine

error was determined using a standard (GFS Chemicals Calcium Carbonate Standard—ACS), which was assayed to be 99.95%–100.05% $CaCO_3$. This standard was measured several times during each analytical session to check instrument performance. Selected samples were run in replicates, as well. For some Site 884 samples, the sample counts were lower than the blank counts, resulting in negative %$CaCO_3$. We treated these data as zero %$CaCO_3$.

Carbonate accumulation rates (CARs) were calculated as described in Lyle et al. (2005). First, we needed dry bulk density (DBD; g/cm³) values. Because no high-resolution DBD measurements were available for the sites considered, we estimated the DBD from the wet bulk density (WBD) based on physical property measurements of discreet samples using site-specific linear regression equations. For the sites considered, R^2 was 0.90 or better. Because there were many more available measurements for wet bulk density based on shipboard gamma ray attenuation (GRA or GRAPE) than on discreet sample physical property analysis, we then correlated GRA(PE) and WBD data using site-specific linear regression equations. To build these equations, we used GRA data collected at the same depth (or within 5 cm) of the measured WBD based on physical properties. For the sites considered, R^2 was 0.68 or better, with two exceptions (Site 929, $R^2 = 0.17$; Site 748, $R^2 = 0.37$) for which CAR calculations carry some uncertainty (see also the Discussion section below). The sites-specific regression equations were used to calculate DBD starting from GRA data collected at the same depth (or within 5 cm) of %$CaCO_3$ samples. We emphasize that these relationships were built using all available data from the same site hole as our $CaCO_3$ samples, with the exception of Site 1263. At this site, the correlation between DBD and WBD and between GRA and WBD were built using data from Site 1263 Hole A, as no bulk and dry density data were available from Hole B (the hole used in this study). We do not think that this approach biased our results, as Site 1263 Holes A and B were drilled only ∼20 m apart (Shipboard Scientific Party, 2004a). However, to confirm this, we compared the GRA data from Site 1263 Holes A and B, following the approach of Reghellin et al. (2013) (Figure S2 in Supporting Information S1). This comparison highlighted the sediment similarity between the two holes, further supporting our approach.

Second, we calculated mass accumulation rates (MARs; mg/cm² kyr) by multiplying the DBD with the linear sedimentation rate (cm/kyr) determined for each sample as follows:

$$\text{Linear sedimentation rate} \left(\frac{\text{cm}}{\text{kyr}} \right) = \frac{\left(\text{sample depth} \left(\text{m} \right) - \text{shallower sample depth} \left(\text{m} \right) \right) * 100}{\left(\text{sample age} \left(\text{Ma} \right) - \text{shallower sample age} \left(\text{Ma} \right) \right) * 1000}$$

Finally, CARs were determined by multiplying MARs with the sample $CaCO_3$ weight percent (%$CaCO_3$). In some cases, we obtained negative CAR values due to negative GRA density values and/or calculated dry bulk density values. This was the case for a few samples from Sites 884, 1090, and U1404. We removed these samples from each site data set.

For Sites 689, 699, 748, 844, 929, 1053, 1090, 1263, U1404, and U1406, GRA(PE), WBD, DBD, and, when needed %$CaCO_3$, data were retrieved from online data repositories (https://www.ngdc.noaa.gov/mgg/curator/data/joides_resolution; http://iodp.tamu.edu/janusweb/links/links_all.shtml).

The approach described above was used to calculate CARs at every site included in this study with the exception of Sites 709, 711, and 1218, for which we used published data (Pälike et al., 2012; Peterson & Backman, 1990). We note that at these sites, the DBD was calculated using a different approach compared to ours. Specifically, at Sites 709 and 711, measured DBD of samples analyzed for %$CaCO_3$ was used when available. When not available, an averaged DBD value samples adjacent to the ones analyzed for %$CaCO_3$ was utilized instead. At these sites, we did not apply the approach we used for all the other sites because the R^2 for the Site 709 GRA versus WBD correlation was below 0.02 and there were no GRA data available for Site 711 samples deeper than ∼56 mbsf (meters below seafloor; middle Eocene-early Oligocene samples were located between 124 and 215 mbsf). The Sites 709 and 711 linear sedimentation rates, MARs, and CARs included in this study are different from the published ones (Peterson & Backman, 1990) because we recalculated the sample ages according to the 2012 Geological Time Scale (Figure S3 in Supporting Information S1). At Site 1218, DBD calculations were based on lithology rather than on equations built using all the data available from one site (Lyle et al., 2005). We used the DBD provided (Pälike et al., 2012) because this approach yielded more precise results at Site 1218 and the difference in the calculation of DBD (and thus MAR) at Site 1218 did not significantly affect our data interpretation. In fact, if we were to use the same approach we used to calculate the DBD at the other sites included in this study, at Site 1218 DBD values would have been 7% lower (Lyle et al., 2005), but the CARs general trend would have

remained the same. For Site 1218 also, the linear sedimentation rates, MARs, and CARs calculated for this study are different from the published ones (Pälike et al., 2012) because we recalculated the sample ages according to the 2012 Geological Time Scale (Figure S4 in Supporting Information S1).

3. Results

Analysis of middle and late Eocene sedimentary records from the equatorial Pacific and Atlantic Oceans showed several CAEs (CAEs 1–7; Table S14 in Supporting Information S1; Lyle et al., 2005; Pälike et al., 2012). Compared to Site 1218, our data show that Site 884 recorded higher CARs than Site 1218 that fluctuated during the time period investigated. Specifically, Site 884 recorded CARs ~1,000 mg/cm^2 kyr and higher ~36.5–35.5 Ma and then again starting from ~34.7 Ma (Figure 2a).

In the North Atlantic Ocean, Site U1406 CARs remained relatively stable (average value ~420 mg/cm^2 kyr), whereas Site U1404 recorded fluctuating CARs (values between ~0 and ~390 mg/cm^2 kyr) (Figure 2b). Site 1053 recorded CARs >2,000 mg/cm^2 kyr from 38.6 until 35 Ma, with peaks at ~38, ~37.5, ~36.3, ~35.8, and ~35 Ma, whereas the western equatorial Atlantic Site 929 showed CARs >1,500 mg/cm^2 kyr ~41, ~37, ~35, and at the E/O boundary (Figure 2b).

In the South Atlantic Ocean, Site 1090 recorded a fluctuation in CARs from ~42.2–37 Ma (Figure 2c). Interestingly, high CARs at Site 1090–42.2–42 Ma resemble a coeval peak in CARs at Sites 748 and 929 (Figures 2b and 2e), though the low resolution of the available data sets may not fully constrain the magnitude and duration of the event at these sites. At Site 1263, CAR values were higher in the middle Eocene compared to the late Eocene (averaged values ~1,334 mg/cm^2 kyr vs. ~852 mg/cm^2 kyr, respectively), with peaks at ~39.7, ~39.4–39, and ~35–34 Ma (Figure 2c). In the sub-Antarctic Atlantic Ocean, Site 699 recorded several episodes of high carbonate accumulation, with CARs >500 mg/cm^2 kyr (Figure 2c).

In the Indian Ocean, Sites 709 and 711 recorded fluctuating CARs. In particular, Site 709 recorded CARs between ~256 and 1,494 mg/cm^2 kyr, with higher values ~41.4–41, ~40.4–40.2, ~38.3–38.2, and ~35.2–35 Ma. At Site 711, CARs oscillated between ~0 and 866 mg/cm^2 kyr, with intervals of virtually no CaCO$_3$ preserved ~39–38.5 and ~37 Ma and short intervals with relatively high CAR ~38.3–38.2 and ~35.2–35 Ma, coeval with the ones at Site 709 (Figure 2d).

In the Southern Ocean, Site 689 recorded an increase in CARs at ~41 Ma, ~37.4, and ~37 Ma, whereas Site 748 CARs increased ~41 and ~37 Ma and at the E/O boundary (values >1,700; >1,000; >700 mg/cm^2 kyr, respectively) (Figure 2e).

4. Discussion

Carbonate surface production, dissolution, and dilution by other sediment types are the processes that influence accumulation of CaCO$_3$ sediments at any specific location (Broecker & Peng, 1982; Sarmiento & Gruber, 2006). In general, CaCO$_3$ stability decreases at lower temperatures and, most importantly, at deeper water depths, although it is also a function of organic matter respiration. At the seafloor, the CaCO$_3$ content of sediments can be affected by the saturation state of bottom waters, dilution by non-CaCO$_3$ material, and dissolution driven by organic carbon remineralization and consequent pore water acidification (Broecker & Peng, 1982; Sarmiento & Gruber, 2006).

The reconstruction of global CaCO$_3$ fluxes at the seafloor and their variation through time represents an important step to understand changes in weathering and other geochemical cycles, whereas regional changes of CaCO$_3$ burial provide the opportunity to assess the impacts of changes in ocean circulation and surface CaCO$_3$ production (Lyle, 2003). However, distinguishing the impact that global versus regional processes had on the middle-late Eocene CaCO$_3$ burial can be challenging. One approach to disentangle the contribution of different processes is the investigation of records from different ocean basin. For example, during the early Cenozoic the Pacific Ocean was bigger than today (Lyle et al., 2008), thus it is possible that it could have recorded a global signal (e.g., change in the lysocline/CCD depth). Instead, in other oceans (e.g., Atlantic), a global signal could have been masked by regional processes, such as changes primary productivity and ocean circulation. Our data suggest that this approach is incorrect because even sedimentary records from the Pacific Ocean (e.g., Site 884; this study), were
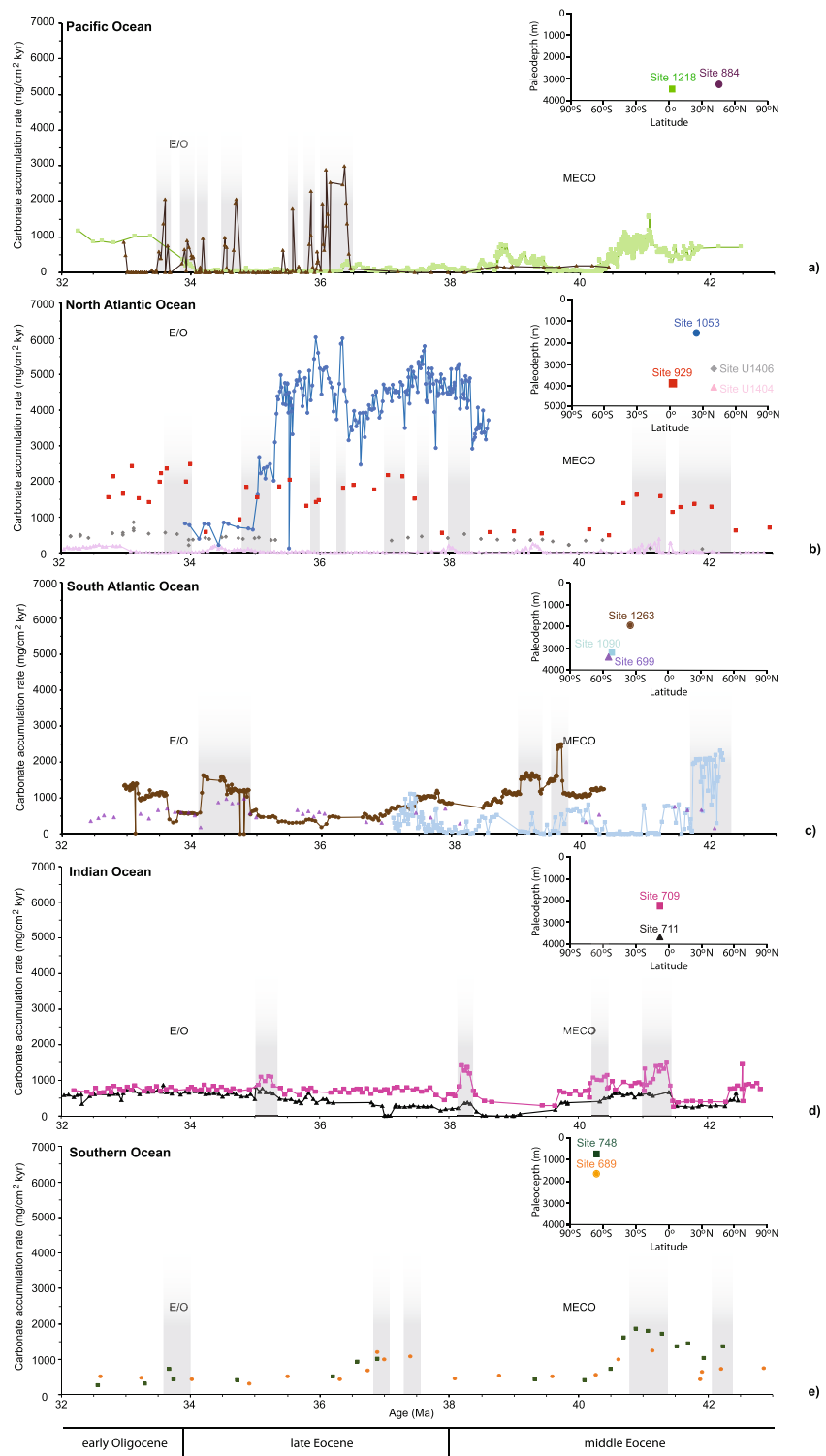
Figure 2. Middle Eocene-early Oligocene carbonate accumulation rates (CARs). (a) Pacific, (b) North Atlantic, (c) South Atlantic, (d) Indian, and (e) Southern Ocean CARs. The CAR peaks discussed in the text are highlighted in gray. E/O = Eocene/Oligocene boundary. MECO = Middle Eocene Climatic Optimum. The insets show paleolatitude and paleodepth of each site included in this study. Data sets characterized by a low temporal resolution are shown as data points only.

affected by regional processes (e.g., fluctuating surface CaCO₃ production). This was already proposed by Lyle et al. (2005) and Rea and Lyle (2005) for the east equatorial Pacific (Leg 199 sites), as well.

In the context of previous studies (Coxall et al., 2005; Pälike et al., 2012; Rea & Lyle, 2005; Tripati et al., 2005), our new high-resolution data sets from the northwestern Pacific and the Atlantic Oceans (Sites 884, 1053, 1263, and 1090), combined with other ODP and IODP records (Figures 1 and 2) show that the magnitude of CaCO₃ accumulation was highly variable and that enhanced CaCO₃ burial was spatially localized.

Comparison of our data with the Eocene CAEs identified by previous studies (Table S14 in Supporting Information S1) supports the hypothesis that high CARs were recorded in different ocean basins (Figure 2), but not the hypothesis that these episodes were global and synchronous events (as proposed by Pälike et al., 2012). It is possible that the low resolution of some of our records (Sites 689, 699, 748, 929, and U1406), together with uncertainties of the age models used, might have influenced this conclusion. In addition, some sites carry more uncertainties compared to others because of the limited data available to calculate CARs (Sites 748 and 929). Even so, some of the deep records included in this study that have sufficient sampling resolution (e.g., Sites 711 and U1404) did not record some of the CAEs. We also note that Griffith et al. (2010) did not find clear CAEs in late Eocene records from the North Pacific (Shatsky Rise), despite peaks in barite accumulation rates. Overall, we think that these lines of evidence indicate that CAEs were not globally synchronous events.

Fluctuations in CARs occurred during long-term global increases in benthic foraminiferal δ¹⁸O (i.e., cooling and increased in ice volume; Cramer et al., 2009; Westerhold et al., 2020; Zachos et al., 2001). Considering that CaCO₃ is more soluble at lower temperatures (e.g., Broecker & Peng, 1982; Zeebe & Wolf-Gladrow, 2001), the decrease in temperature that took place in the middle-late Eocene would have reduced the preservation of CaCO₃ at the seafloor. However, temperature has a rather small effect on carbonate solubility when compared to pressure (e.g., Broecker & Peng, 1982; Zeebe & Wolf-Gladrow, 2001). Thus, we do not think that the middle-late Eocene cooling substantially affected our CAR records.

One of the mechanisms proposed to explain the rapid increase in CaCO₃ preservation ~33.9 Ma involved ice-sheet build-up in Antarctica and decrease in sea level, with consequent shelf-basin CaCO₃ fractionation and higher input of dissolved inorganic carbon and alkalinity delivery to the ocean (Coxall et al., 2005; Merico et al., 2008). Unfortunately, the temporal resolution of some of our records, in addition to the uncertainties of the age models, do not allow us to make a meaningful comparison between sea-level changes (e.g., Kominz et al., 2008; Miller et al., 2020) and middle to late Eocene CARs, so to test if shelf-basin fractionation could have been a reasonable explanation of our results. However, we note that higher CARs at times of higher benthic foraminiferal δ¹⁸O values were interpreted at Sites 1218 and 1219 as a possible link among increased CaCO₃ preservation at the seafloor, cooling, and possibly initial, ephemeral glaciations (Lyle et al., 2005).

Our data show that high CARs are also a characteristic of sedimentary records located at different paleodepths and geological settings (Figures 1 and 2; Tables 1 and 2), suggesting that the middle-late Eocene geographic and bathymetric heterogeneity in CaCO₃ accumulation was heavily influenced by local processes (i.e., primary productivity and changes in ocean circulation). Interestingly, high CARs at Sites 1053 and 884 coincide with lower CARs at every other location investigated (Figure 2). We propose that these sites are examples of "hot spots" (cf. Sosdian et al., 2018)—locations where high surface CaCO₃ production is preserved at the seafloor, resulting in higher than average CaCO₃ burial flux. The hot spot idea was proposed to explain the shift in the ocean's CaCO₃ burial between the Atlantic and the equatorial Pacific during the interglacial and glacial stages of the late Pleistocene. In this context, the input of calcium and bicarbonate ions delivered to the ocean by rivers was balanced by enhanced CaCO₃ burial in limited areas (Sosdian et al., 2018).

In general, CaCO₃ burial is promoted by the presence of deep water mass that is not corrosive to calcite (e.g., Broecker & Peng, 1982; Ridgwell & Zeebe, 2005; Sarmiento & Gruber, 2006; Zeebe & Wolf-Gladrow, 2001). However, in regions characterized by a high CaCO₃ supply, CaCO₃ burial is possible even in the presence of undersaturated waters (Dunne et al., 2012). In this scenario, lower CARs at sites other than Sites 884 and 1053 could have been a compensatory mechanism for the high CaCO₃ burial in the northwestern Atlantic and Pacific Oceans. At this time, the hot spot hypothesis is speculative because the records included in this study do not allow us to draw a firm conclusion about the representativeness of the areas around Sites 884 and 1053. Are the areas characterized by the CARs at these sites truly large enough to have an impact on the CaCO₃ budget for the whole

Table 2
Geological Setting and Core Lithological Information for All the Sites Included in This Study

Site	Geological setting	Major lithologies	Calcareous fossil preservation
ODP Site 884B	Detroit Seamount, Meiji Drift deposition began by the late Eocene/earliest Oligocene	Claystone with minor nannofossil chalk (604.8–694.7 mbsf); chalk, claystone, ash layers with soft sediment deformation & intraformational clasts (694.7–771 mbsf)	Calcareous nannoplankton—moderate preservation; benthic foraminifera—moderate to poor preservation
ODP Site 1053A	top of Blake Nose Escarpment, located on the Blake Plateau (oceanic plateau)	Clayey ooze with foraminifera, nannofossil ooze to siliceous nannofossil ooze, siliceous nannofossil chalk (0–182.73 mbsf)	Calcareous nannoplankton—moderately to well preserved; Foraminifera—well preserved
ODP Site 1090B	southern flank of Agulhas Ridge (oceanic ridge)	Mud-bearing diatom ooze, mud- and diatom-bearing nannofossil ooze and chalk (69.41–351.59 mcd); mud-bearing nannofossil ooze and chalk (351.59–409.49 mcd)	Calcareous nannoplankton—good to medium preservation; planktonic foraminifera—rare, poor to moderate preservation; benthic foraminifera—moderately well preserved.
ODP Site 1263B	located just below crest of Walvis Ridge (aseismic ridge)	Nannofossil ooze, foraminifera-bearing nannofossil ooze, chalky nannofossil ooze (53.3–99.1 mcd).	Nannofossils—moderate to good preservation; foraminifera—good preservation
ODP Site 689B	near crest of Maud Rise (oceanic plateau)	Nannofossil ooze, diatom-bearing nannofossil ooze (72.1–149.1 mbsf); semilithified ooze to chalk, including foraminiferal nannofossil ooze and nannofossil ooze (149.1–236.3 mbsf)	Calcareous nannoplankton—moderate preservation; foraminifera—good to excellent preservation
ODP Site 699A	SE slope of North Georgia Rise (oceanic plateau)	Siliceous nannofossil ooze, nannofossil ooze (243.1–335.43 mbsf); nannofossil chalk (335.43–375.19 mbsf)	Calcareous nannoplankton and foraminifera—well—preserved
ODP Site 709C	lies in a small basin perched near the summit of Madingley Rise, a regional topographic high between Carlsberg Ridge and northern Mascarene Plateau	Nannofossil ooze and chalk, alternating with clay-bearing nannofossil ooze and chalk (117.90–353.70 mbsf).	Calcareous nannoplankton—good to moderately good preservation; foraminifera—fairly well preserved.
ODP Site 711A	northern edge of the Madingley Rise	Nannofossil ooze, clay-bearing nannofossil ooze, clayey nannofossil ooze (68.0–173.0 mbsf); clay-bearing nannofossil chalk, clay- and radiolarian-bearing nannofossil chalk, clay-bearing radiolarian ooze (173.0–249.6 mbsf)	Calcareous nannoplankton—well preserved; foraminifera—moderately well preserved.
ODP Site 748B	Western Raggatt Basin on southern Kerguelen Plateau (oceanic plateau)	Nannofossil ooze with occasional biogenic silica debris (10.2–180.6 mbsf)	Calcareous nannoplankton—well preserved; foraminifera—excellent preservation
ODP Site 929E	north flank of Ceara Rise (aseismic rise)	Nannofossil chalk and clayey nannofossil mixed with sedimentary rock, both with trace to moderate amounts of biosiliceous material (440–520 mbsf); clayey nannofossil limestone and clayey nannofossil mixed with sedimentary rock (520–670 mbsf)	Calcareous nannoplankton—well or moderately preserved; planktonic foraminifera—poor preservation; benthic foraminifera—moderate to good preservation
ODP Site 1218	central tropical Pacific north of Clipperton Fracture Zone (subsidizing middle ocean ridge)	Lower portion is nannofossil ooze grading down to nannofossil chalk with minor amounts of radiolarians and up to 50% (A-52.1–216.9 mbsf; B-51.0–215.6 mbsf; C-55.0–218.5 mbsf); (A-216.9–250.2 mbsf; B - 215.6–249.0 mbsf; C-218.5–252.2 mbsf)—interlayered radiolarite and nannofossil chalk, each with variable amounts of clay (up to 30%)	Calcareous nannofossils—well preserved with intervals of dissolution; planktonic foraminifera—occasional dissolution—resistant species are present in poor conditions; benthic foraminifera—moderate preservation
IODP Site U1404A	J-Anomaly Ridge drift deposit	Clayey/silty nannofossil ooze, nannofossil ooze (200.62–226.50 mbsf); clay/claystone and radiolarian clay with variable amounts of radiolarians and nannofossils (226.50–299.82 mbsf).	Calcareous nannofossils—poor to good preservation. Foraminifera—poor to good preservation

Table 2
Continued

Site	Geological setting	Major lithologies	Calcareous fossil preservation
IODP Site U1406A	J-Anomaly Ridge drift deposit	Nannofossil chalk with foraminifera (184.86–243.40 mbsf);	Calcareous nannofossils—moderate to good preservation; foraminifera— moderate to very good preservation

Note. mobs = meters below seafloor; mcd = meters composite depth; ODP = Ocean Drilling Program; IODP = Integrated Ocean Drilling Program. For each site, the information included in this table were retrieved from the ODP/IODP Site report (terminology is reproduced from each report, and therefore is not uniform among all sites). See Table 1 for specific references.

ocean? The investigation of surface productivity proxies from Sites 884 and 1053 as well as additional high-resolution deep-sea sedimentary records, will be fundamental to confirming this hypothesis in future studies.

4.1. The Role of Surface Carbonate Production in Driving Middle-Late Eocene CARs in Sediments Shallower Than 2,500 m

The middle-late Eocene sedimentary record at Site 689 (Southern Ocean) is characterized by relatively high CARs at ~41 Ma and ~37 Ma. At this time, sediments were predominantly (diatom-bearing) nannofossil ooze (Table 2). In the Sub-Antarctic Indian Ocean, Site 748 recorded high CARs between ~42.3–41 Ma, which resulted in deposition of nannofossil ooze (Table 2). Carbonates remained the main type of sediment until the E/O boundary, when siliceous fossils increased (Schumacher & Lazarus, 2004). The equatorial Indian Ocean Site 709 recorded several episodes of high CARs between ~41 and 35 Ma, as reflected in the lithology of the cores analyzed (nannofossil ooze and chalk alternating with clay-bearing nannofossil ooze and chalk; Table 2) (Figure 2c; Figure S5k in Supporting Information S1).

Site 1263 records fluctuating CARs from ~40-33 Ma, with two main high CAR episodes ~39.7 and ~34–35 Ma (Figure 2c; Figure S5g in Supporting Information S1). Three data points show a rapid decrease and recovery in %$CaCO_3$ values. However, replicate analysis of these samples indicate that the low %$CaCO_3$ values are an analytical artifact. At this site, the %$CaCO_3$ remain relatively constant, whereas MARs varied throughout the studied interval (Figure S5g in Supporting Information S1) pointing to a variable, although high, supply of $CaCO_3$ from the ocean surface as the main driver of the CAR record. The lithology at this site ([foraminifera-bearing] nannofossil ooze to chalky nannofossil ooze; Table 2) support this interpretation. In addition, the good preservation of foraminifera and calcareous nannofossil indicate the absence of corrosive water masses at this location. Interestingly, an increase in MARs driven mainly by $CaCO_3$ deposition was found at deeper sites drilled during ODP Leg 208 on Walvis Ridge (Shipboard Scientific Party, 2004a). In particular, Site 1266 recorded higher MARs in the late Eocene, whereas Sites 1267 and 1262 were characterized by an increase in MARs at the E/O boundary. However, at these sites the presence of unconformities, condensed upper and middle Eocene sections, downslope transport, and limited %$CaCO_3$ data available through the ODP repository (Shipboard Scientific Party, 2004c, 2004d, 2004e) prevented us from thoroughly evaluating changes in CARs at these sites ~43-34 Ma.

At Site 1053 (northwestern Atlantic), high $CaCO_3$ surface productivity was recorded in the lithology of almost the entire sedimentary record at Hole A (siliceous nannofossil ooze and chalk; Table 2). The drop in MARs starting ~35 Ma (Figure S5e in Supporting Information S1) might be an artifact of a decrease in linear sedimentation rate due to the arbitrary age assignment to the top of the section (Borrelli et al., 2014) or it might be a true signal (see below). We note that even if we were to use a different age model to calculate MARs and CARs at Site 1053 (e.g., age model by Katz et al. (2011), Figure S6 in Supporting Information S1), the drop in mass accumulation rates in the late late Eocene would still be present, possibly indicating a true signal. For this study, we used the age model by Borrelli et al. (2014) instead of Katz et al. (2011), which was based on biostratigraphy datums from the original site report (Shipboard Scientific Party, 1998), because of the strong agreement between the arbitrary age assignment to the top of the section and other biostratigraphic datums (HO *Cribrocentrum reticulatum*, *Turborotalia pomeroli*, *Globigerinatheka semiinvoluta*). In addition, the arbitrary age assignment to the top of the section by Borrelli and colleagues provided the context for the interpretation of Chron C15n boundaries. See Borrelli et al. (2014) for a detailed discussion regarding the Site 1053 age model.
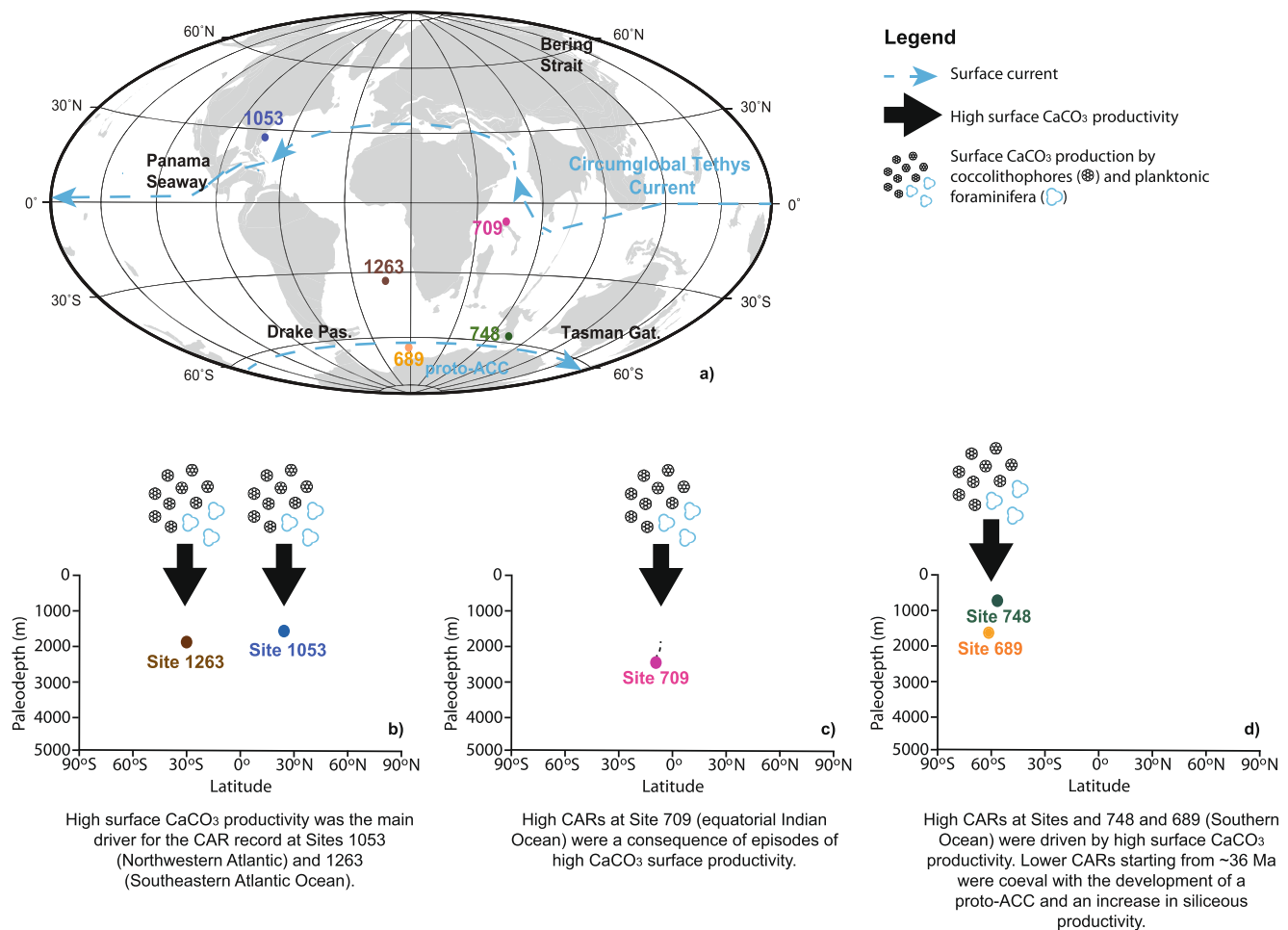
Figure 3. Summary of the processes influencing carbonate accumulation rates (CARs) at sites located at paleodepth ≤2,500 m. (a) Approximate paleolocation of the shallower sites used in this study. Surface currents that can potentially have impacted our records are highlighted in blue (after Borrelli et al., 2014; Hotinski & Toggweiler, 2003; Katz et al., 2011). Proto-ACC = proto Antarctic Circumpolar Current, as defined by Borrelli et al. (2014). The base map was generated from http://www.odsn.de. (b) Processes influencing CAR records in the Atlantic Ocean. (c) Processes influencing CAR records in the Indian Ocean. The dashed line indicates the Site 709 subsidence during the time of this study. (d) Processes influencing CAR records in the Southern Ocean.

Mass accumulation rate or %$CaCO_3$ alone are not good proxies to reconstruct changes in the $CaCO_3$ cycle (Lyle, 2003), but the comparison between MARs and %$CaCO_3$ in the context of CARs can provide insight into the processes responsible for the $CaCO_3$ records. At sites located at paleodepths shallower than 2,500 m, our data show that high CARs were driven by high MARs rather than changes in %$CaCO_3$ (Figures 2b, 2d and 2e; Figures S5e, S5g, and S5k–S5m in Supporting Information S1), which indicates increased $CaCO_3$ surface production (as supported by the lithologies of Sites 689, 709, 748, 1053, and 1263) rather than a change in the $CaCO_3$ preservation at the seafloor (Figure 3), as also supported by the calcareous microfossil (calcareous nannoplankton and foraminifera) preservation at these locations, which ranged from moderate to excellent (Table 2). This is not surprising considering the depth of our shallower sites, which makes them less susceptible to variations in bottom water chemistry (i.e., changes in dissolved inorganic content of the ocean and alkalinity). Site 709 deepened ~400 m from the middle Eocene to the late Eocene (cf. Figure S1 of Bohaty et al., 2009). However this change in depth did not affect the CAR record. This conclusion is in agreement with Peterson and Backman's (1990), as they found no indication of drastic changes in $CaCO_3$ surface production and/or $CaCO_3$ dissolution during the middle and late Eocene at Site 709, despite some variability in the data.

The analysis of sediments from the equatorial Pacific (Sites 1218 and 1219) revealed very low Eocene organic carbon MARs compared to the expected ones based on the location of the studied sites and compared to the Eocene biogenic barium, a proxy reflecting export production (Olivarez Lyle & Lyle, 2006). The apparent

discrepancy between higher surface productivity and low burial of organic matter is explained by efficient remineralization of organic carbon in the water column and/or at the sediment-water interface until ~40 Ma (John et al., 2013; Olivarez Lyle & Lyle, 2005, 2006). Based on this, it is possible that CARs at Sites 689, 709, 748, 1053, and 1263 might have been influenced by higher dissolution in the water column and/or at the sediment/water interface. However, the middle and late Eocene is also a time of decrease in temperature. Boscolo-Galazzo et al. (2018) proposed a temperature-dependent biological pump. In their context, cooler waters would have allowed more organic matter to reach the seafloor. Regardless of the cooling that took place in the middle and late Eocene, modeling simulations showed that respiration-driven $CaCO_3$ dissolution is not very efficient at depths characterized by supersaturated bottom waters (e.g., Dunne et al., 2012), like at our shallower sites.

Overall, our reconstructions support the hypothesis that strong longitudinal and latitudinal differences existed in the production of $CaCO_3$ during the Eocene (Lyle et al., 2005). The role of increased $CaCO_3$ production at the surface in driving high CARs at depths ≤2,500 m is perhaps to be expected. However, analysis of sites located at ~3,000–4,000 m paleodepth in the equatorial Pacific showed that some of the Eocene CAEs were associated with pulses of surface $CaCO_3$ productivity (Griffith et al., 2010; Lyle et al., 2005; Rea & Lyle, 2005).

Based on our data sets, we propose that the heterogeneity in $CaCO_3$ production in the middle and late Eocene was a consequence of local changes in ocean circulation consequent to the opening of the Drake Passage and of the Tasman Gateway. According to modeling simulations, the opening of the Drake Passage changed the ocean nutrient distribution through changes in ocean circulation affecting upwelling (Ladant et al., 2018). At Sites 689, 748, and 709 higher CARs were recorded between ~41 and ~37 Ma. This time coincides with the spreading of the Dove Basin (a deep basin located in the Southern Scotia Sea) and a minor deepening of the Tasman Gateway (Livermore et al., 2007; Stickley et al., 2004). Starting from ~36 Ma, lower CARs were coeval with the progressive deepening of the Tasman Gateway (Stickley et al., 2004) and development of a proto-Antarctic Circumpolar Current (Borrelli et al., 2014). This decrease in $CaCO_3$ accumulation is consistent with modeling simulations (Ladant et al., 2018). In fact, it was shown that an open Drake Passage caused lower nutrient availability at low latitudes and higher nutrient availability at the high latitudes of the Southern Ocean (Ladant et al., 2018). This shift in nutrient availability caused a decrease in productivity at low latitudes and an increase in siliceous productivity at high latitudes of the Southern Ocean, in agreement with several proxy reconstructions (e.g., Diester-Haass, 1991; Diester-Haass & Zahn, 1996, 2001; Egan et al., 2013; Nilsen et al., 2003; Plancq et al., 2014; Salamy & Zachos, 1999; Schumacher & Lazarus, 2004; Siesser, 1995).

At Site 1053 high CARs were recorded until ~35 Ma. In the middle and late Eocene, high productivity was recorded at equatorial locations (e.g., Griffith et al., 2010; Lyle et al., 2005; Wagner, 2002). In this case, it is possible that the effects of an open Drake Passage were counterbalanced by upwelling near the equator associated with the (reduced) circumglobal Tethys current (Hotinski & Toggweiler, 2003) and transport of these nutrients at sites located north and south of the equator via Ekman transport. The importance of this mechanism became negligible once the Tethys Seaway closed ~35 Ma (Allen & Armstrong, 2008), possibly explaining the drop in Site 1053 CARs around this time. However, if the Tethys Seaway was still open in the late Eocene (e.g., Hutchison et al., 2018), the Site 1053 sedimentary record could have been influenced by nondeposition or persistent erosion from the late Eocene to the present, as proposed in the site report (Shipboard Scientific Party, 1998).

Coccolithophore calcification rates are higher at higher carbonate ion concentrations (Riebesell et al., 2000). Thus, it is possible that our records could be explained by enhanced surface $CaCO_3$ productivity promoted by higher alkalinity input to the ocean, rather than by nutrient reorganization. Weathering fluxes were relatively stable or slightly lower during the middle and late Eocene (Caves et al., 2016; Lear et al., 2003), although some studies proposed an increase in weathering in the late Eocene-early Oligocene (e.g., Basak & Martin, 2013; Coxall et al., 2005; Ravizza & Peucker-Ehrenbrink, 2003; Raymo & Ruddiman, 1992; Zachos et al., 1999). Our data do not allow us to draw a firm conclusion regarding the role of changes in nutrient supply and alkalinity in driving $CaCO_3$ accumulation and burial at the seafloor, but we note that high CARs were recorded in middle Eocene sediments, when the alkalinity input was presumably stable or slightly lower compared to the late Eocene. This suggests that alkalinity input alone was not enough to stimulate episodes of high surface $CaCO_3$ productivity. Although it is possible that both higher alkalinity delivery to the ocean and nutrient redistribution acted in concert to stimulate calcareous phytoplankton productivity at least for part of our record, changes in upwelling might have had a more prominent role (Lyle et al., 2005, 2008).

Increased deposition of calcium carbonate from the middle Eocene to the early Oligocene characterize also the Tasmanian offshore region, as shown by some of the sites drilled during Leg 189 (Sites 1170, 1171, and 1172; Shipboard Scientific Party, 2001a). In this case, the change in deposition from (glauconitic) siliciclastic sediments to carbonates was associated with a rapid deepening from neritic to middle bathyal depths (from 50–100 m to up to 1,000 m) and was driven by an increased productivity and ocean ventilation (Shipboard Scientific Party, 2001a, 2001b, 2001c, 2001d).

To summarize, we propose that the middle-late Eocene CARs at sites located at depths shallower than or around 2,500 m in the Atlantic, sub-Antarctic, Southern, and Indian Oceans were a consequence of $CaCO_3$ surface production mainly driven by ocean circulation changes consequent to the opening of the Drake Passage and Tasman Gateway (Figure 3). However, we note that this conclusion carries some uncertainties, in particular considering the lack of a definitive understanding of which processes regulate surface $CaCO_3$ productivity today.

4.2. The Role of Surface Carbonate Production and Ocean Ventilation in Driving Middle-Late Eocene CARs in Sediments Deeper Than 2,500 m

A latitudinal and paleodepth difference in CARs was recorded in the Pacific Ocean. In fact, the equatorial Pacific recorded fluctuations in CARs ∼42.5–34 Ma (cf. CAEs as reported in Lyle et al., 2005 and Pälike et al., 2012), whereas the northwestern Pacific did not (Site 884; Figure 2a; Figure S5a in Supporting Information S1). Site 1218 is a very interesting site. It was located at the middle Eocene equator, in an area of high productivity (Shipboard Scientific Party, 2002). Thus, surface $CaCO_3$ production played an important role in the CAR record of this site (Lyle et al., 2005; Rea & Lyle, 2005). Pälike et al. (2012) explored CAEs in more detail and concluded that they represented fluctuations of the CCD during the middle and late Eocene due to the quality (labile vs. refractory) and amount of organic carbon reaching the sediments, possibly in conjunction with changes in weathering. It is worth noting that Site 1218 experienced a ∼1,000 m of subsidence from the middle to the late Eocene (Rea & Lyle, 2005). Although it was suggested that deep water formation occurred both in the North Pacific and in the Southern Ocean during most of the Eocene (e.g., Baatsen, von der Heydt, Huber, et al., 2018; Baatsen, von der Heydt, Kliphuis, et al., 2018; Hutchison et al., 2018, 2019; McKinley et al., 2019; Thomas, 2004; Thomas et al., 2008, 2014), ε_{Nd} data identified a deep water mass originating from the Southern Ocean as the main water mass bathing the tropical Pacific after ∼42–45 Ma (Hague et al., 2012; Thomas et al., 2008). Thus, subsidence at Site 1218 would not have moved it into a different deep water mass.

At Site 884, very low CARs were recorded until ∼38.5 Ma and were driven mostly by lower MARs, suggesting low surface $CaCO_3$ production. Between ∼38 and ∼37 Ma, Site 884 was characterized by very low MARs and zero %$CaCO_3$. The absence of $CaCO_3$ in late Eocene sediments could be a consequence of a change in productivity or in dissolution following deposition. Episodes of extremely low %$CaCO_3$ punctuated the Site 884 record also between ∼36 and ∼34, possibly indicating fluctuating surface $CaCO_3$ production or $CaCO_3$ preservation at the seafloor. The calcareous microfossil preservation ranging from moderate to poor support the latter hypothesis.

In the Atlantic Ocean, Site U1404 clearly shows fluctuations in $CaCO_3$ preservation, as also supported by the lithology and the calcareous microfossil preservation at this site (Figure 2b; Figure S5d in Supporting Information S1; Table 2). Interestingly, these fluctuations are similar to those recorded in the equatorial Pacific (Figure 2a). Sites U1406, 929, and 699 did not record a decrease in $CaCO_3$ preservation at this time, as supported by the lithology and preservation of nannoplankton and foraminifera (Table 2). Site 1090 recorded episodes of high $CaCO_3$ accumulation, but also poor $CaCO_3$ preservation (Figure 2b; Figures S5c, S5f, S5h, and S5i in Supporting Information S1). At this site, $CaCO_3$ export production was an important mechanism in driving $CaCO_3$ accumulation until ∼40.5 Ma, when $CaCO_3$ preservation might have been affected by changes in post-depositional dissolution (Diekmann et al., 2004).

In the Indian Ocean, Site 711 experienced episodes of dissolution at ∼39–38.5 and ∼37 Ma (Figure 2c; Figure S5j in Supporting Information S1). This decrease in $CaCO_3$ preservation in the equatorial Indian Ocean at depths <3,400 m was confirmed by the presence of radiolarian-rich sediments at Site 711 during this time (Peterson & Backman, 1990). Starting ∼37 Ma, higher CARs were again recorded at Site 711 and were supposedly related to the "traditional" deepening of the CCD at the E/O boundary (Peterson & Backman, 1990; Peterson et al., 1992; Van Andel, 1975), even if the changes at Site 711 preceded the CCD deepening in the equatorial Pacific (Coxall et al., 2005; Pälike et al., 2012) by several million years. It is worth noting that Site 711 recorded

a few small peaks in CARs, which were coeval with those recorded at Site 709. We interpret this as evidence of short episodes of higher surface CaCO$_3$ productivity. Site 711 also experienced ∼300 m of subsidence from the middle Eocene to the early Oligocene (cf. Figure S1 of Bohaty et al., 2009). We do not think that this change in depth influenced the CAR record at this site for two reasons. First, CaCO$_3$ preservation improved in the younger part of the record, when the site was deeper. If subsidence had a significant influence on the CaCO$_3$ burial, we would have expected lower CAR values in the younger part of the record compared to the older, which is not the case. Second, the change in paleodepth at Site 711 did not affect the water mass bathing this site, as explained more in detail below.

At sites located deeper than 2,500 m, chemical compensation (set of conditions affecting the CaCO$_3$ saturation state and, therefore, CaCO$_3$ dissolution and preservation at the seafloor; Boudreau et al., 2018) influence the amount of CaCO$_3$ that can be buried in sediments. In fact, an increase in CaCO$_3$ dissolution has a higher impact in areas characterized by low (vs. high) CaCO$_3$ rain to the seafloor (Lyle et al., 2005). However, surface productivity also can affect chemical compensation because a decrease/increase in surface CaCO$_3$ calcification can cause an increase/decrease in surface water alkalinity and a transfer of this signal to deeper depths via sinking and deepwater formation (i.e., biological carbonate compensation; Boudreau et al., 2018). For instance, changes in coccolithophore productivity influenced deep-sea CaCO$_3$ burial during the late Neogene (Si & Rosenthal, 2019). However, in light of the data from our shallower sites, we do not think that a drop in marine plankton calcification is a likely explanation of our deeper records.

Modeling simulations showed an increase in deep ocean carbonate ion concentration, as well as an increase in calcium and carbonate ion production during the middle and late Eocene (∼43-34 Ma; Boudreau & Luo, 2017). Higher concentrations of carbonate ion in deep waters could be explained by higher weathering rates, which are not supported by modeling simulations and proxy reconstructions for the middle and early late Eocene (Caves et al., 2016; Lear et al., 2003). Even so, several of our deeper sites recorded increasing CARs in the late Eocene. Based on this, we suggest that the increase in the carbonate ion concentration was not geographically homogenous. This could be a consequence of a different distribution of carbonate ion among different basins, in particular considering that calcium and carbonate concentrations at saturation do not vary substantially among basins (Sarmiento & Gruber, 2006).

As summarized by Hutchison et al. (2018), late Eocene (∼38 Ma) paleogeography strongly influenced ocean circulation. In particular, an open but shallow Drake Passage and Tasman Gateway only allowed for a weak Antarctic Circumpolar Current to flow eastward (proto-ACC; Borrelli et al., 2014). At the same time, the equatorial Atlantic and Pacific were connected by an open Panama seaway, whereas the northern Pacific Ocean was isolated from the Arctic Ocean because of a closed Bering Strait. On the other hand, a bidirectional flow of water between the Atlantic and Arctic Oceans was made possible by the presence of narrow and shallow gateways. Finally, in the late Eocene, the Tethys Ocean was still connected to the Indian and Atlantic Ocean, as well as with the Arctic Ocean via the Turgai Strait. This different paleogeography translated to a different deep ocean circulation pattern compared to today. We think that the middle-late Eocene ocean circulation pattern contributed to different CaCO$_3$ burial at sites deeper than 2,500 m. More specifically, we propose that the heterogeneity in the carbonate ion concentration among different basins was a consequence of the different water masses bathing the different sites included in this study.

In the northwestern Pacific (Site 884), the overall increase in CARs at ∼36.5 Ma was coeval with a change in ocean circulation and a water mass originating from the Southern Ocean (Borrelli & Katz, 2015) or, possibly, from the North Pacific (Baatsen, von der Heydt, Huber, et al., 2018; Baatsen, von der Heydt, Kliphuis, et al., 2018; Hutchison et al., 2019, 2018; McKinley et al., 2019). Our data hint at a reduction in CARs in the northwestern Pacific after the E/O boundary. If the North Pacific was a source of deep water in the late Eocene (Baatsen, von der Heydt, Huber, et al., 2018; Baatsen, von der Heydt, Kliphuis, et al., 2018; Hutchison et al., 2019, 2018; McKinley et al., 2019), then the sedimentary record might have been affected by a change in the source region of the deep water mass bathing Site 884, and a consequent change from a well-ventilated to a poorly ventilated area. This is in agreement with modeling simulations showing that the initiation of sinking in the North Atlantic coincided with the cessation of sinking in the North Pacific (Hutchison et al., 2019). Additional late Eocene/early Oligocene data from Site 884 and other deep locations in the North Pacific are necessary to further investigate this scenario.

In the northeastern Atlantic (Site U1404), a drop in MARs and a slow increase in %CaCO$_3$ starting ~38 Ma coincided with a first pulse of Northern Component Water (NCW) originating from the Labrador Sea (Borrelli et al., 2014) but this interpretation does not agree with modeling simulations and analysis of other sedimentary records. In fact, modeling simulation did not show formation of deep water in the North Atlantic at ~38 Ma due to the influence of fresh surface water flowing from the Arctic Ocean into the high latitudes of the North Atlantic (Hutchison et al., 2018, 2019). The analysis of several North Atlantic proxy records agreed with this scenario as they showed that NCW export to the northwestern Atlantic did not start before ~36 Ma (Coxall et al., 2018). However, the presence of contourite sediment deposits in the Faeroe-Shetland Basin and offshore Newfoundland were interpreted as evidence that deep water flow originated in the North Atlantic starting from the early to middle Eocene (~49-47 Ma; Boyle et al., 2017; Hohbein et al., 2012), possibly as a consequence of a deep enough Greenland-Scotland Ridge (depth >200 m) when the Arctic Ocean and the North Atlantic were not connected (Vahlenkamp et al., 2018). Taking into account the uncertainties related to the reconstructions of the initiation of deep water formation in the North Atlantic and considering that Site 1404 was drilled on a drift deposit, it is possible that the CaCO$_3$ record could have been influenced by the high clay supply to this site (Norris et al., 2014c) or by current winnowing. We note that these processes could have influenced the Site U1406 record, as well.

No drastic changes in ocean circulation were reported for the sub-Antarctic Atlantic Ocean (Site 699) (Via & Thomas, 2006), which we propose remained well-ventilated, based on the nannofossil and foraminiferal preservation (Table 2). In contrast, neodymium (Nd) isotopes showed that the Sub-Antarctic Atlantic Ocean (Site 1090) started to be influenced by Pacific waters entering the Atlantic sector of the Southern Ocean through an opened Drake Passage and sinking in the Weddell Sea during periods of deep water formation during the middle and late Eocene (Scher & Martin, 2006). It is possible that this influx of Pacific deep water affected CaCO$_3$ preservation at Site 1090. Future studies involving high-resolution benthic foraminiferal stable isotope data will help to refine our understanding of ocean circulation at Site 1090 and its possible role in CaCO$_3$ burial at this site during the middle-late Eocene.

Overall, the deeper sedimentary records included in this study reveal that CaCO$_3$ preservation did not increase globally during the middle-late Eocene. Different trends in CaCO$_3$ burial at Sites 884, U1404, 699, and 1090 and comparison of these trends with ocean circulation reconstructions and modeling (Baatsen, von der Heydt, Huber, et al., 2018; Baatsen, von der Heydt, Kliphuis, et al., 2018; Borrelli et al., 2014; Borrelli & Katz, 2015; Hutchison et al., 2019, 2018; Langton et al., 2016; McKinley et al., 2019; Scher & Martin, 2006) suggest a possible link between CaCO$_3$ preservation at the seafloor and ocean circulation changes (or absence thereof) (Figure 4). This hypothesis is in agreement with Miller et al. (2009), who argued for a connection between an increase in thermohaline circulation and deep-sea ventilation and increased CaCO$_3$ preservation at deeper depths at the E/O boundary. Although intriguing, this hypothesis remains speculative because only some of the deeper water records included in this study can be explained by a change in ventilation. For example, Nd isotopes showed a single water mass from the Southern Ocean bathing the tropical Pacific starting from ~45-42 Ma (Hague et al., 2012; Thomas et al., 2008), but the Site 1218 CARs continued to fluctuate until the E/O boundary. Considering that during the Eocene Site 1218 was located in an area of upwelling and that the nannofossil ooze and chalk are an important component of the sedimentary record (Shipboard Scientific Party, 2002), we think that surface CaCO$_3$ production played a significant role in driving the middle and late Eocene CAR record, as also proposed by Lyle et al. (2005) and Rea and Lyle (2005) (Figure 4).

Site 711 is another example of a site recording a substantial change in CAR, but not a significant change in ocean circulation. In fact, ε_{Nd} records from Ninetyeast Ridge (Site 757) indicate that this region was bathed by intermediate to deep waters that originated in the Southern Ocean (Martin & Scher, 2006). The similarity of the Site 757 ε_{Nd} record with the one from Site 1090 (sub-Antarctic Atlantic Ocean, Scher & Martin, 2006) indicates that in the middle-late Eocene water mass were flowing from the Atlantic sector of the Atlantic ocean to the Indian Ocean at intermediate and deeper depths, similar to what happens today (Martin & Scher, 2006). Based on these findings, it seems that Site 711 did not experience a substantial change in ocean circulation during the middle and late Eocene. This is supported by benthic foraminiferal carbon isotope data indicating a young and nutrient-depleted water mass bathing the Indian Ocean at bottom depths during this time (Zachos et al., 1992).
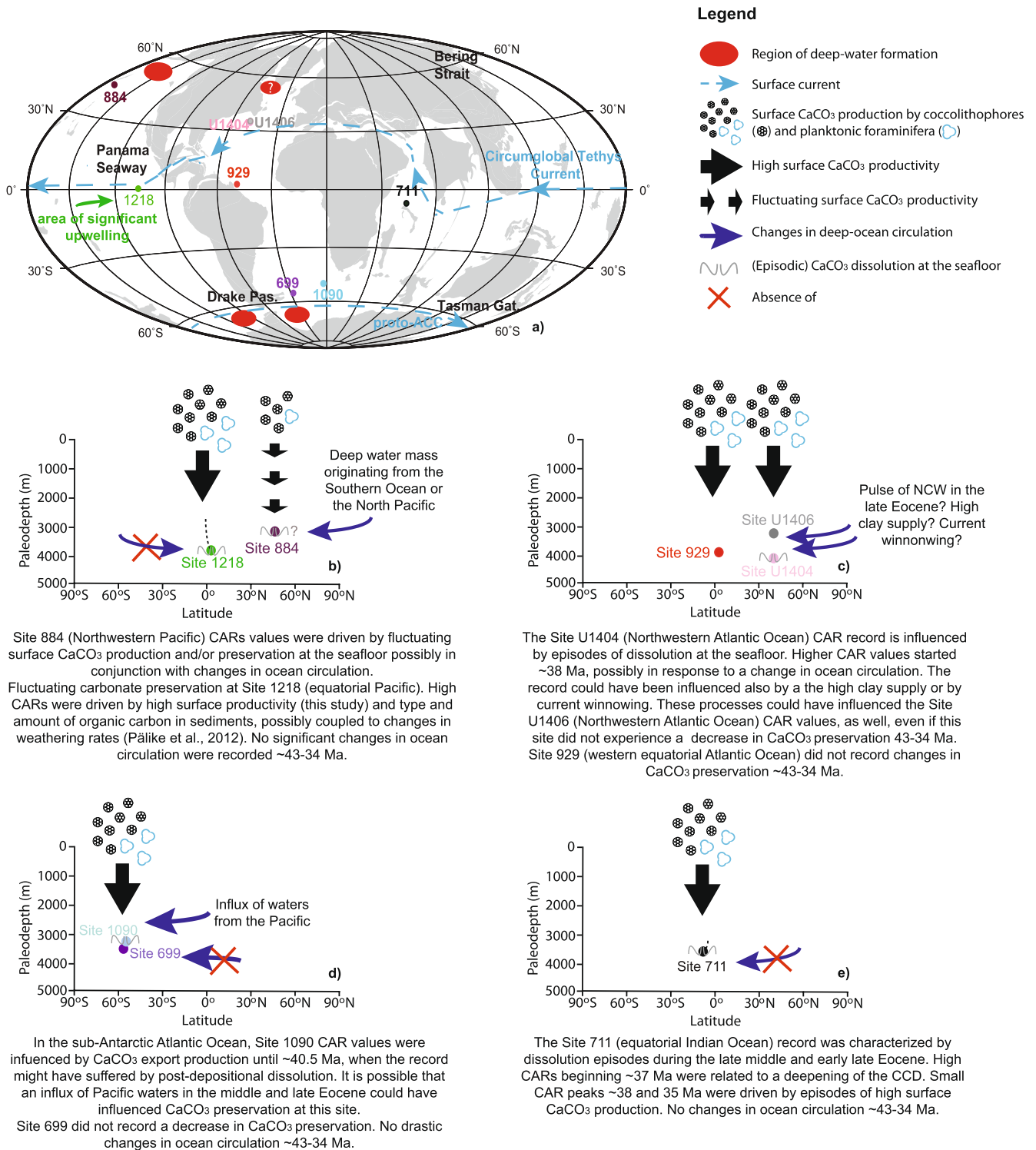
Figure 4. Summary of the processes influencing carbonate accumulation rates (CARs) at sites located at paleodepths >2,500 m. (a) Approximate paleolocation of the deeper sites used in this study. Surface currents that can potentially have impacted our records are highlighted in blue (after Borrelli et al., 2014; Hotinski & Toggweiler, 2003; Katz et al., 2011). Proto-ACC = proto Antarctic Circumpolar Current, as defined by Borrelli et al. (2014). The red circles represent regions of deep-water formation based on Baatsen, von der Heydt, Huber, et al. (2018); Baatsen, von der Heydt, Kliphuis, et al. (2018), Borrelli et al. (2014), Hutchison et al. (2018), and McKinley et al. (2019). The base map was generated from http://www.odsn.de. (b) Processes influencing CAR records in the Pacific Ocean. (c) Processes influencing CAR records in the North Atlantic Ocean. (d) Processes influencing CAR records in the South Atlantic Ocean. (e) Processes influencing CAR records in the equatorial Indian Ocean. The dashed line indicates site subsidence (when subsidence occurred in a significant manner) during the time of this study. CCD = carbonate compensation depth; NCW = Northern Component Water.

5. Conclusions

In this study, we compared carbonate accumulation rates of sites located in different basins, geological settings, and at different paleodepths to test the hypothesis that $CaCO_3$ burial was heterogeneous during the middle and late Eocene (~43-34 Ma). Our results show to a highly variable $CaCO_3$ preservation during this time, pointing to a combination of processes that influenced the sedimentary record. Specifically, we propose that surface $CaCO_3$ production drove $CaCO_3$ accumulation in sediments shallower than (or around) 2,500 m. Instead, an increase in $CaCO_3$ preservation at deeper sites could have been triggered by surface $CaCO_3$ production in conjunction with an increase in ventilation caused by changes in ocean circulation driven by tectonic movements. The comparison of our CARs with ocean circulation reconstructions support this scenario, at least for the Atlantic Ocean and the northwestern Pacific Ocean. Considering that the Eocene oceanic gateways, basins widths, and overturning geometries were very different compared to today and that this could have influenced the regional ocean-climate-productivity-marine chemistry interactions, our study highlights the need to investigate sites located in different oceans and geological settings to gain a better understanding of the evolution of the carbonate cycle at the onset of the greenhouse-icehouse transition.

Conflict of Interest

The authors declare no conflicts of interest relevant to this study

Data Availability Statement

Open research: All data sets generated for this study are available on Pangaea (https://doi.pangaea.de/10.1594/PANGAEA.934247). For Sites 689, 699, 748, 844, 929, 1053, 1090, 1263, U1404, and U1406, GRA(PE), WBD, DBD, and, when needed %$CaCO_3$, data were retrieved from online data repositories (https://www.ngdc.noaa.gov/mgg/curator/data/joides_resolution; http://iodp.tamu.edu/janusweb/links/links_all.shtml).

References

Abelson, M., Agnon, A., & Almogi-Labin, A. (2008). Indications for control of the Iceland plume on the Eocene-Oligocene 'greenhouse-icehouse" climate transition. *Earth and Planetary Science Letters*, *265*(1–2), 33–48. https://doi.org/10.1016/j.epsl.2007.09.021

Abelson, M., & Erez, J. (2017). The onset of modern-like Atlantic meridional overturning circulation at the Eocene-Oligocene transition: Evidence, causes, and possible implications for global cooling. *Geochemistry, Geophysics, Geosystems*, *18*(6), 2177–2199. https://doi.org/10.1002/2017GC006826

Allen, M. B., & Armstrong, H. A. (2008). Arabia-Eurasia collision and the forcing of mid-Cenozoic global cooling. *Palaeogeography, Palaeoclimatology, Palaeoecology*, *265*(1–2), 52–58. https://doi.org/10.1016/j.palaeo.2008.04.021

Anagnostou, E., John, E. H., Babila, T. L., Sexton, P. F., Ridgwell, A., Lunt, D. J., et al. (2020). Proxy evidence for state-dependence of climate sensitivity in the Eocene greenhouse. *Nature Communications*, *11*, 4436. https://doi.org/10.1038/s41467-020-17887-x

Anagnostou, E., John, E. H., Edgar, K. M., Foster, G. L., Ridgwell, A., Inglis, G. N., et al. (2016). Changing atmospheric CO_2 concentration was the primary driver of early Cenozoic climate. *Nature*, *533*, 380–384. https://doi.org/10.1038/nature17423

Armstrong McKay, D. I., Tyrrell, T., & Wilson, P. A. (2016). Global carbon cycle perturbation across the Eocene-Oligocene climate transition. *Paleoceanography*, *31*, 311–329. https://doi.org/10.1002/2015PA002818

Aubry, M.-P., & Bord, D. (2009). Reshuffling the cards in the photic zone at the Eocene/Oligocene boundary. In C. Koeberl, & A. Montanari (Eds.), *The late Eocene Earth—Hothouse, icehouse, and impacts* (pp. 279–301). Geological Society of America. https://doi.org/10.1130/2009.2452(18)

Baatsen, M., van Hinsbergen, D. J. J., von der Heydt, A. S., Dijkstra, H. A., Sluijs, A., Abels, H. A., & Bijl, P. K. (2016). Reconstructing geographical boundary conditions for paleoclimate modelling during the Cenozoic. *Climate of the Past*, *12*, 1635–1644. https://doi.org/10.5194/cp-12-1635-2016

Baatsen, M., von der Heydt, A. S., Huber, M., Kliphuis, M. A., Bijl, P. K., Sluijs, A., & Dijkstra, H. A. (2018). *Equilibrium state and sensitivity of the simulated middle-to-late Eocene climate*. Climate of the Past Discussion. [preprint]. https://doi.org/10.5194/cp-2018-43

Baatsen, M., von der Heydt, A. S., Kliphuis, M. A., Viebahn, J., & Dijkstra, H. A. (2018). Multiple states in the late Eocene ocean circulation. *Global and Planetary Change*, *163*, 18–28. https://doi.org/10.1016/j.gloplacha.2018.02.009

Balch, W. M., & Kilpatrick, K. (1996). Calcification rates in the equatorial Pacific along 140°W. *Deep-Sea Research II*, *43*(4–6), 971–993. https://doi.org/10.1016/0967-0645(96)00032-1

Basak, C., & Martin, E. E. (2013). Antarctic weathering and carbonate compensation at the Eocene-Oligocene transition. *Nature Geoscience*, *6*(2), 121–124. https://doi.org/10.1038/ngeo1707

Berelson, W. M., Balch, W. M., Najjar, R., Feely, R. A., Sabine, C., & Lee, K. (2007). Relating estimates of CaCO3 production, export, and dissolution in the water column to measurements of CaCO3 rain into sediment traps and dissolution on the sea floor: A revised global carbonate budget. *Global Biogeochemical Cycles*, *21*, GB1024. https://doi.org/10.1029/2006GB002803

Berner, R. A. (1999). A new look at the long-term carbon cycle. *Geological Society of America Today*, *9*(11), 1–6.

Berner, R. A., & Caldeira, K. (1997). The need for mass balance and feedback in the geochemical carbon cycle. *Geology*, *25*(10), 9552–9956. https://doi.org/10.1130/0091-7613(1997)025<0955:tnfmba>2.3.co;2

Bohaty, S. M., & Zachos, J. C. (2003). Significant Southern Ocean warming event in the late middle Eocene. *Geology*, *31*(11), 1017–1020. https://doi.org/10.1130/G19800.1

Bohaty, S. M., Zachos, J. C., Florindo, F., & Delaney, M. L. (2009). Coupled greenhouse warming and deep-sea acidification in the middle Eocene. *Paleoceanography*, *24*, PA2207. https://doi.org/10.1029/2008PA001676

Borrelli, C., Cramer, B. S., & Katz, M. E. (2014). Bipolar Atlantic deepwater circulation in the middle-late Eocene: Effects of Southern Ocean gateway openings. *Paleoceanography*, *29*(4), 308–327. https://doi.org/10.1002/2012PA002444

Borrelli, C., & Katz, M. E. (2015). Dynamic deep-water circulation in the northwestern Pacific during the Eocene: Evidence from Ocean Drilling Program Site 884 benthic foraminiferal stable isotopes ($\delta^{18}O$ and $\delta^{13}C$). *Geosphere*, *11*(4), 1204–1255. https://doi.org/10.1130/GES01152.1

Boscolo-Galazzo, F., Crichton, K. A., Barker, S., & Pearson, P. N. (2018). Temperature dependency of metabolic rates in the upper ocean: A positive feedback to global climate change? *Global and Planetary Change*, *170*, 201–212. https://doi.org/10.1016/j.gloplacha.2018.08.017

Boudreau, B. P., & Luo, Y. (2017). Retrodiction of secular variations in deep-sea $CaCO_3$ burial during the Cenozoic. *Earth and Planetary Science Letters*, *474*, 1–12. https://doi.org/10.1016/j.epsl.2017.06.005

Boudreau, B. P., Middelburg, J. J., & Luo, Y. (2018). The role of calcification in carbonate compensation. *Nature Geoscience*, *11*(12), 894–900. https://doi.org/10.1038/s41561-018-0259-5

Boyle, P. R., Romans, B. W., Tucholke, B. E., Norris, R. D., Swift, S. A., & Sexton, P. F. (2017). Cenozoic North Atlantic deep circulation history recorded in countourite drifts, offshore Newfoundland, Canada. *Marine Geology*, *385*, 185–203. https://doi.org/10.1016/j.margeo.2016.12.014

Brand, L. E. (1994). Physiological ecology of marine coccolithophores. In A. Winter, & W. G. Siesser (Eds.), *Coccolithophores* (pp. 39–49). Cambridge University Press.

Broecker, W. S., & Peng, T.-H. (1982). *Tracers in the sea*. Lamont Doherty Geological Observatory, Columbia University.

Broecker, W. S., & Peng, T.-H. (1987). The role of $CaCO_3$ compensation in the glacial to interglacial atmospheric CO_2 change. *Global Biogeochemical Cycles*, *1*(1), 15–29. https://doi.org/10.1029/GB001i001p00015

Broecker, W. S., & Sanyal, A. (1998). Does atmospheric CO_2 police the rate of chemical weathering? *Global Biogeochemical Cycles*, *12*(3), 403–408. https://doi.org/10.1029/98GB01927

Caves, J. K., Jost, A. B., Lau, K. V., & Maher, K. (2016). Cenozoic carbon cycle imbalances and a variable weathering feedback. *Earth and Planetary Science Letters*, *450*, 152–163. https://doi.org/10.1016/j.epsl.2016.06.035

Channell, J. E. T., Galeotti, S., Billups, K., & Scher, H. (2003). Eocene to Miocene magnetostratigraphy, biostratigraphy, and chemostratigraphy at ODP Site 1090 (Sub-Antarctic South Atlantic). *The Geological Society of America Bulletin*, *115*(5), 607–623. https://doi.org/10.1130/0016-7606(2003)115<0607:etmmba>2.0.co;2:ETMMBA>2.0.CO;2

Cliftt, P. D., Turner, J. & Ocean Drilling Program Leg 152 Scientific Party. (1995). Dynamic support by the Icelandic plume and vertical tectonics of the northeast Atlantic continental margins. *Journal of Geophysical Research: Solid Earth*, *100*(B12), 24473–24486. https://doi.org/10.1029/95JB02511

Coxall, H. K., Huck, C. E., Huber, M., Lear, C. H., Legarda-Lisarri, A., O'Regan, M., et al. (2018). Export of nutrient rich Northern Component Water preceded early Oligocene Antarctic glaciation. *Nature Geoscience*, *11*(3), 190–196. https://doi.org/10.1038/s41561-018-0069-9

Coxall, H. K., Wilson, P. A., Pälike, H., Lear, C. H., & Backman, J. (2005). Rapid stepwise onset of Antarctic glaciation and deeper calcite compensation in the Pacific Ocean. *Nature*, *433*(7021), 53–57. https://doi.org/10.1038/nature03135

Cramer, B. S., Miller, K. G., Barrett, P. J., & Wright, J. D. (2011). Late Cretaceous-Neogene trends in deep ocean temperature and continental ice volume: Reconciling records of benthic foraminiferal geochemistry ($\delta^{18}O$ and Mg/Ca) with sea level history. *Journal of Geophysical Research*, *116*(C12), C12023. https://doi.org/10.1029/2011JC007255

Cramer, B. S., Toggweiler, J. R., Wright, J. D., Katz, M. E., & Miller, K. G. (2009). Ocean overturning since the Late Cretaceous: Inferences from a new benthic foraminiferal isotope compilation. *Paleoceanography*, *24*(4), PA4216. https://doi.org/10.1029/2008PA001683

Cramwinckel, M. J., Huber, M., Kocken, I. J., Agnini, C., Bijl, P. K., Bohaty, S. M., et al. (2018). Synchronous tropical and polar temperature evolution in the Eocene. *Nature*, *559*, 382–386. https://doi.org/10.1038/s41586-018-0272-2

DeConto, R. M., & Pollard, D. (2003). Rapid Cenozoic glaciation of Antarctica induced by declining atmospheric CO_2. *Nature*, *421*(6920), 245–249. https://doi.org/10.1038/nature01290

Diekmann, B., Kuhn, G., Gersonde, R., & Mackensen, A. (2004). Middle Eocene to early Miocene environmental changes in the sub-Antarctic Southern Ocean: Evidence from biogenic and terrigenous depositional patterns at ODP Site 1090. *Global and Planetary Change*, *40*(3–4), 295–313. https://doi.org/10.1016/j.gloplacha.2003.09.001

Diester-Haass, L. (1991). Eocene/Oligocene paleoceanography in the Antarctic Ocean, Atlantic sector (Maud Rise, ODP Leg 113, Site 689B and 690B). *Marine Geology*, *100*(1–4), 249–276. https://doi.org/10.1016/0025-3227(91)90235-V

Diester-Haass, L., & Zahn, R. (1996). Eocene-Oligocene transition in the Southern Ocean: History of water mass circulation and biological productivity. *Geology*, *24*, 163–166. https://doi.org/10.1130/0091-7613(1996)024<0163:EOTITS>2.3.CO;2

Diester-Haass, L., & Zahn, R. (2001). Paleoproductivty increase at the Eocene-Oligocene climatic transition: ODP/DSDP sites 763 and 592. *Palaeogeography, Palaeoclimatology, Palaeoecology*, *172*(1-2), 153–170. https://doi.org/10.1016/S0031-0182(01)00280-2

Dunne, J. P., Hales, B., & Toggweiler, J. R. (2012). Global calcite cycling constrained by sediment preservation controls. *Global Biogeochemical Cycles*, *26*(3), GB3023. https://doi.org/10.1029/2010GB003935

Egan, K. E., Rickaby, R. E. M., Hendry, K. R., & Halliday, A. N. (2013). Opening of the gateways for diatoms primes Earth for Antarctic glaciation. *Earth and Planetary Science Letters*, *375*, 34–43. https://doi.org/10.1016/j.epsl.2013.04.030

Foster, G. L., Royer, D. L., & Lunt, D. J. (2017). Future climate forcing potentially without precedent in the last 420 million years. *Nature Communications*, *8*(1), 14845. https://doi.org/10.1038/ncomms14845

Gradstein, F. M., Ogg, J. G., Schmitz, M. D., & Ogg, G. (2012). *The geological time scale 2012*. Elsevier.

Griffith, E., Calhoun, M., Thomas, E., Averyt, K., Erhardt, A., Bralower, T., et al. (2010). Export productivity and carbonate accumulation in the Pacific Basin at the transition from a greenhouse to icehouse climate (late Eocene to early Oligocene). *Paleoceanography*, *25*(3), PA3212. https://doi.org/10.1029/2010PA001932

Hague, A. M., Thomas, D. J., Huber, M., Korty, R., Woodard, S. C., & Jones, L. B. (2012). Convection of North Pacific deep water during the early Cenozoic. *Geology*, *40*(6), 527–530. https://doi.org/10.1130/G32886.1

Hohbein, M. W., Sexton, P. F., & Cartwright, J. A. (2012). Onset of North Atlantic Deep Water production coincident with inception of the Cenozoic global cooling trend. *Geology*, *40*(3), 255–258. https://doi.org/10.1130/g32461.1

Hotinski, R. M., & Toggweiler, J. R. (2003). Impact of a Tethyan circumglobal passage on ocean heat transport and "equable" climates. *Paleoceanography*, *18*(1), 1007. https://doi.org/10.1029/2001PA000730

Hutchison, D. K., Coxall, H., Lunt, D. J., Steinthorsdottir, M., de Boer, A. M., Baatsen, M., et al. (2021). The Eocene-Oligocene transition: A review of marine and terrestrial proxy data, models, and model-data comparisons. *Climate of the Past*, *17*, 269–315. https://doi.org/10.5194/cp-17-269-2021

Hutchison, D. K., Coxall, H., O'Regan, M., Nilsson, J., Caballero, R., & de Boer, A. M. (2019). Arctic closure as a trigger for Atlantic overturning at the Eocene-Oligocene Transition. *Nature Communications*, *10*, 3797. https://doi.org/10.1038/s41467-019-11828-z

Hutchison, D. K., de Boer, A. M., Coxall, H., Caballero, R., Nilsson, J., & Baatsen, M. (2018). Climate sensitivity and meridional overturning circulation in the late Eocene using GFDL CM2.1. *Climate of the Past*, *14*, 789–810. https://doi.org/10.5194/cp-14-789-2018

Iglesias-Rodriguez, M. D., Armstrong, R., FeelyHood, R. R., Kleypas, J., Milliman, J. D., et al. (2002). Progress made in study of ocean's calcium carbonate budget. *EOS*, *83*(34). https://doi.org/10.1029/2002EO000267

John, E., Pearson, P. N., Birch, H. B., Coxall, H. K., Wade, B. S., & Foster, G. L. (2013). Warm ocean processes and carbon cycling in the Eocene. *Philosophical Transactions of the Royal Society A*, *371*(2001), 20130099. https://doi.org/10.1098/rsta.2013.0099

Katz, M. E., Cramer, B. S., Toggweiler, J. R., Esmay, G., Liu, C., Miller, K. G., et al. (2011). Impact of Antarctic Circumpolar Current development on late Paleogene ocean structure. *Science*, *332*(6033), 1076–1079. https://doi.org/10.1126/science.1202122

Katz, M. E., Miller, K. G., Wright, J. D., Wade, B. S., Browning, J. V., Cramer, B. S., & Rosenthal, Y. (2008). Stepwise transition from the Eocene greenhouse to the Oligocene icehouse. *Nature Geoscience*, *1*(5), 329–334. https://doi.org/10.1038/ngeo179

Kominz, M. A., Browning, J. V., Miller, K. G., Sugarman, P. J., Mizintseva, S., & Scotese, C. R. (2008). Late Cretaceous to Miocene sea-level estimates from the New Jersey Delaware coastal plain coreholes: An error analysis. *Basin Research*, *20*(2), 211–226. https://doi.org/10.1111/j.1365-2117.2008.00354.x

Kordesch, W. S., Bohaty, S. M., Pälike, H., Wilson, P. A., Edgar, K. M., Agnini, C., et al. (2015). *Dynamic, large magnitude CCD changes in the Atlantic during the middle Eocene climatic Optimum*. Paper presented at the American Geophysical Union Fall Meeting.

Ladant, J.-B., Donnadieu, Y., Bopp, L., Lear, C. H., & Wilson, P. A. (2018). Meridional contrasts in productivity changes driven by the opening of Drake Passage. *Paleoceanography and Paleoclimatology*, *33*(3), 302–317. https://doi.org/10.1002/2017PA003211

Langton, S. J., Rabideaux, N. M., Borrelli, C., & Katz, M. E. (2016). Southeastern Atlantic deepwater evolution during the late middle Eocene to earliest Oligocene (ODP Site 1263 and DSDP Site 366). *Geosphere*, *12*(3), 1032–1047. https://doi.org/10.1130/GES01268.1

Lear, C. H., Bailey, T. R., Pearson, P. H., Coxall, H. K., & Rosenthal, Y. (2008). Cooling and ice-sheet growth across the Eocene-Oligocene transition. *Geology*, *36*(3), 251–254. https://doi.org/10.1130/G24584A.1

Lear, C. H., Elderfield, H., & Wilson, P. A. (2003). A Cenozoic seawater Sr/Ca record from benthic foraminiferal calcite and its application in determining global weathering fluxes. *Earth and Planetary Science Letters*, *208*(1-2), 69–84. https://doi.org/10.1016/S0012-821X(02)01156-1

Liu, Z., Pagani, M., Zanniker, D., DeConto, R., Huber, M., Brinkhuis, H., et al. (2009). Global cooling during the Eocene-Oligocene climate transition. *Science*, *323*(5918), 1187–1190. https://doi.org/10.1126/science.1166368

Livermore, R., Hillenbrand, C.-D., Meredith, M., & Eagles, G. (2007). Drake Passage and Cenozoic climate: An open and shut case? *Geochemistry, Geophysics, Geosystems*, *8*(1), Q01005. https://doi.org/10.1029/2005GC001224

Lyle, M. (2003). Neogene carbonate burial in the Pacific Ocean. *Paleoceanography*, *18*(3), 1059. https://doi.org/10.1029/2002PA000777

Lyle, M., Barron, J., Bralower, T. J., Huber, M., Olivarez Lyle, A., Ravelo, A. C., et al. (2008). Pacific Ocean and Cenozoic evolution of climate. *Reviews of Geophysics*, *46*(2), RG2002. https://doi.org/10.1029/2005RG000190

Lyle, M. W., Olivarez Lyle, A., Backman, J., & Tripati, A. (2005). Biogenic sedimentation in the Eocene equatorial Pacific—The stuttering greenhouse and Eocene carbonate compensation depth. In P. Wilson, M. W. Lyle, & J. Firth (Eds.), *Proceedings of the Ocean Drilling Program scientific results* (Vol. 199, pp. 1–35). Ocean Drilling Program.

Marino, M., & Flores, J.-A. (2002). Middle Eocene to early Oligocene calcareous nannofossil stratigraphy at Leg 177 Site 1090. *Marine Micropaleontology*, *45*(3-4), 383–398. https://doi.org/10.1016/S0377-8398(02)00036-1

Martin, E. F., & Scher, H. (2006). A Nd isotopic study of southern sourced waters and Indonesian Throughflow at intermediate depths in the Cenozoic Indian Ocean. *Geochemistry, Geophysics, Geosystems*, *7*(9), Q09N02. https://doi.org/10.1029/2006GC001302

Martin, W. R., & Sayles, F. L. (1996). $CaCO_3$ dissolution in sediments of the Ceara Rise, western equatorial Atlantic. *Geochmica et Cosmochimica Acta*, *60*(2), 243–263. https://doi.org/10.1016/0016-7037(95)00383-5

McKinley, C., Thomas, D. J., LeVay, L. J., & Rolewicz, Z. (2019). Nd isotopic structure of the Pacific ocean 40-10 Ma, and evidence for the reorganization of the deep North Pacific Ocean circulation between 36 and 25 Ma. *Earth and Planetary Science Letters*, *521*, 139–149. https://doi.org/10.1016/j.epsl.2019.06.009

Mead, G. A., Hodell, D. A., & Ciesielski, P. F. (1993). Late Eocene to Oligocene vertical oxygen isotopic gradients in the South Atlantic: Implications for warm saline deep water. In J. P. Kennett, & D. A. Warnke (Eds.), *The Antarctic paleoenvironment: A perspective on global change: Part 2, Antarctic research series* (Vol. 60, pp. 27–48). American Geophysical Union.

Merico, A., Tyrrell, T., & Wilson, P. A. (2008). Eocene/Oligocene ocean de-acidification linked to Antarctic glaciation by sea-level fall. *Nature*, *452*(7190), 979–983. https://doi.org/10.1038/nature06853

Miller, K. G., Browing, J. V., Schmelz, W. J., Kopp, R. E., Mountain, G. S., & Wright, J. D. (2020). Cenozoic sea-level and cryospheric evolution from deep-sea geochemical and continental margin records. *Science Advances*, *6*(20), eaaz1346. https://doi.org/10.1126/sciadv.aaz1346

Miller, K. G., Browning, J. V., Aubry, M.-P., Wade, B. S., Katz, M. E., Kulpecz, A. A., & Wright, J. D. (2008). Eocene-Oligocene global climate and sea-level changes: St. Stephens Quarry, Alabama. *The Geological Society of America Bulletin*, *120*(1-2), 34–53. https://doi.org/10.1130/B26105.1

Miller, K. G., Wright, J. D., Katz, M. E., Wade, B. S., Browning, J. V., Cramer, B. S., et al. (2009). Climate threshold at the Eocene-Oligocene transition: Antarctic ice sheet influence on ocean circulation. In C. Koeberl, & A. Montanari (Eds.), *The late Eocene Earth—Hothouse, icehouse, and impacts* (Vol. 452, pp. 169–178). Geological Society of America. https://doi.org/10.1130/2009.2452(11)

Milliman, J. D., Troy, P. J., Balch, W. M., Adams, A. K., Li, Y.-H., & Mackenzi, F. T. (1999). Biologically mediated dissolution of calcium carbonate above the chemical lysocline? *Deep-Sea Research I*, *46*(10), 1653–1669. https://doi.org/10.1016/S0967-0637(99)00034-5

Nilsen, E. B., Anderson, L. D., & Delaney, M. L. (2003). Paleoproductivity, nutrient burial, climate change and the carbon cycle in the western equatorial Atlantic across the Eocene/Oligocene boundary. *Paleoceanography*, *18*(3), 1057. https://doi.org/10.1029/2002PA000804

Norris, R. D., Wilson, P. A., Blum, P., Fehr, A., Agnini, C., Bornemann, A., et al. (2014a). Site U1404. In R. D. Norris, P. A. Wilson, P. Blum (Eds.), & the Expedition 342 Scientists. (Eds.), *Proceedings of the international ocean discovery program* (Vol. 342, pp. 1–97). Integrated Ocean Drilling Program.

Norris, R. D., Wilson, P. A., Blum, P., Fehr, A., Agnini, C., Bornemann, A., et al. (2014b). Site U1406. In R. D. Norris, P. A. Wilson, P. Blum (Eds.), & the Expedition 342 Scientists. (Eds.), *Proceedings of the international ocean discovery program* (Vol. 342, pp. 1–99). Integrated Ocean Drilling Program.

Norris, R. D., Wilson, P. A., Blum, P., Fehr, A., Agnini, C., Bornemann, A., et al. (2014c). Expedition 342 summary. In R. D. Norris, P. A. Wilson, P. Blum (Eds.), & the Expedition 342 Scientists. (Eds.), *Proceedings of the international ocean discovery Program* (Vol. 342, pp. 1–99). Integrated Ocean Drilling Program. https://doi.org/10.2204/iodp.proc.342.101.2014

Olivarez Lyle, A., & Lyle, M. (2005). Organic carbon and barium in Eocene sediments: Possible controls on nutrient recycling in the Eocene equatorial Pacific. In P. Wilson, M. W. Lyle, & J. Firth (Eds.), *Proceedings of the Ocean Drilling Program scientific results* (Vol. 199, pp. 1–33). Ocean Drilling Program.

Olivarez Lyle, A., & Lyle, M. W. (2006). Missing organic carbon in Eocene marine sediments: Is metabolism the biological feedback that maintains end-member climates? *Paleoceanography*, *21*, PA2007. https://doi.org/10.1029/2005PA001230

Pagani, M., Huber, M., Liu, Z., Bohaty, S. M., Henderiks, J., Sijp, W., et al. (2011). The role of carbon dioxide during the onset of Antarctic glaciation. *Science*, *334*(6060), 1261–1264. https://doi.org/10.1126/science.1203909

Pak, D. K., & Miller, K. G. (1995). Isotopic and faunal record of Paleogene deep-water transitions in the North Pacific. In D. K. Rea, I. A. Basov, D. W. Scholl, & J. F. Allan (Eds.), *Proceedings of the Ocean Drilling Program scientific results* (Vol. 145, pp. 265–281). Ocean Drilling Program. https://doi.org/10.2973/odp.proc.sr.145.121.1995

Pälike, H., Lyle, M. W., Nishi, H., Raffi, I., Ridgwell, A., Gamage, K., et al. (2012). A Cenozoic record of the equatorial Pacific carbonate compensation depth. *Nature*, *488*(7413), 609–615. https://doi.org/10.1038/nature11360

Pälike, H., Nishi, N., Lyle, M., Raffi, I., Gamage, K., & Klaus, A., & the Expedition 320/321 Scientists. (2010). Expedition 320/321 summary. In H. Pälike, M. Lyle, H. Nishi, I. Raffi, K. Gamage, A. Klaus (Eds.), & Expedition 320/321 Scientists. (Eds.), *Proceedings of the international ocean discovery Program* (Vol. 320/321, pp. 1–141). Integrated Ocean Drilling Program.

Peterson, L. C., & Backman, J. (1990). Late Cenozoic carbonate accumulation and the history of the carbonate compensation depth in the western equatorial Indian Ocean. In R. A. Duncan, & J. Backman (Eds.), *Proceedings of the Ocean Drilling Program scientific results* (Vol. 115, pp. 467–507). Ocean Drilling Program. https://doi.org/10.2973/odp.proc.sr.115.163.1990

Peterson, L. C., Murray, D. W., Ehrmann, W. U., & Hempel, P. (1992). Cenozoic carbonate accumulation and compensation depth changes in the Indian Ocean. In R. A. Duncan, D. K. Rea, R. B. Kidd, U. von Rad, & J. K. Weissel (Eds.), *Synthesis of results from scientific drilling in the Indian Ocean scientific results geophysical monograph series* (Vol. 70, pp. 311–333). American Geophysical Union. https://doi.org/10.1029/GM070p0311

Plancq, J., Mattioli, E., Pittet, B., Simon, L., & Grossi, V. (2014). Productivity and sea-surface temperature changes recorded during the late Eocene-early Oligocene at DSDP Site 511 (South Atlantic). *Paleogeography, Palaeoclimatology, Palaeoecology*, *407*, 34–44. https://doi.org/10.1016/j.palaeo.2014.04.016

Pusz, A. E., Thunell, R. C., & Miller, K. G. (2011). Deep water temperature, carbonate ion, and ice volume changes, across the Eocene-Oligocene transition. *Paleoceanography*, *26*(2), PA2205. https://doi.org/10.1029/2010PA001950

Ravizza, G., & Peucker-Ehrenbrink, B. (2003). The marine ^{187}Os/^{188}Os record of the Eocene-Oligocene transition: The interplay of weathering and glaciation. *Earth and Planetary Science Letters*, *210*(1–2), 151–165. https://doi.org/10.1016/S0012-821X(03)00137-7

Raymo, M. E., & Ruddiman, W. F. (1992). Tectonic forcing of late Cenozoic climate. *Nature*, *359*, 117–122. https://doi.org/10.1038/359117a0

Rea, D. K., & Lyle, M. W. (2005). Paleogene calcite compensation depth in the eastern subtropical Pacific: Answers and questions. *Paleoceanography*, *20*(1), PA1012. https://doi.org/10.1029/2004PA001064

Reghellin, D., Dickens, G., & Backman, J. (2013). The relationship between wet bulk density and carbonate content sediments from the Eastern Equatorial Pacific. *Marine Geology*, *344*, 41–52. https://doi.org/10.1016/j.margeo.2013.07.007

Ridgwell, A., & Zeebe, R. E. (2005). The role of the global carbonate cycle in the regulation and evolution of the Earth system. *Earth and Planetary Science Letters*, *234*(3–4), 299–315. https://doi.org/10.1016/j.epsl.2005.03.006

Riebesell, U., Zondervan, I., Rost, B., Tortell, P. D., Zeebe, R. E., & Morel, F. M. M. (2000). Reduced calcification of marine plankton in response to increased atmospheric CO_2. *Nature*, *407*, 364–367. https://doi.org/10.1038/35030078

Rost, B., & Riebesell, U. (2004). Coccolithophores and the biological pump: Responses to environmental changes. In H. R. Thierstein, & J. R. Young (Eds.), *Coccolithophores: From molecular processes to global impact* (pp. 99–125). Springer. https://doi.org/10.1007/978-3-662-06278-4_5

Salamy, K. A., & Zachos, J. C. (1999). Latest Eocene-Early Oligocene climate change and Southern Ocean fertility: Inferences from sediment accumulation and stable isotope data. *Paleogeography, Palaeoclimatology, Palaeoecology*, *145*(1-3), 61–77. https://doi.org/10.1016/S0031-0182(98)00093-5

Sarmiento, J. L., & Gruber, N. (2006). Calcium carbonate cycle. In *Ocean biogeochemical dynamics* (pp. 359–391). Princeton University Press.

Scher, H. D., & Martin, E. E. (2006). Timing and climatic consequences of the opening of Drake Passage. *Science*, *312*(5772), 428–430. https://doi.org/10.1126/science.1120044

Schumacher, S., & Lazarus, D. (2004). Regional differences in pelagic productivity in the late Eocene to early Oligocene—A comparison of southern high latitudes and lower latitudes. *Paleogeography, Palaeoclimatology, Palaeoecology*, *214*(3), 243–263. https://doi.org/10.1016/s0031-0182(04)00424-9

Scotese, C. R. (2021). An Atlas of Phanerozoic Paleogeographic Maps: The seas comes in and the seas goes out. *Annual Reviews of Earth & Planetary Sciences*, *49*, 669–708. https://doi.org/10.1146/annurev-earth-081320-064052

Shipboard Scientific Party. (1988a). Site 689. In P. F. Barker (Ed.), *Proceedings of the Ocean Drilling Program initial reports* (Vol. 113, pp. 89–181). Ocean Drilling Program.

Shipboard Scientific Party. (1988b). Site 699. In P. F. Ciesielski, & Y. Kristoffersen (Eds.), *Proceedings of the Ocean Drilling Program initial reports* (Vol. 114, pp. 151–254). Ocean Drilling Program.

Shipboard Scientific Party. (1988c). Site 709. In J. Backman (Ed.), *Proceedings of the Ocean Drilling Program initial reports* (Vol. 115, pp. 459–588). Ocean Drilling Program.

Shipboard Scientific Party. (1988d). Site 711. In J. Backman (Ed.), *Proceedings of the Ocean Drilling Program initial reports* (Vol. 115, pp. 657–732). Ocean Drilling Program.

Shipboard Scientific Party. (1989). Site 748. In R. Schlich, & S. W. WiseJr. (Eds.), *Proceedings of the Ocean Drilling Program initial reports* (Vol. 120, pp. 157–235). Ocean Drilling Program.

Shipboard Scientific Party. (1993). Site 884. In D. K. Rea, & I. A. Basov (Eds.), *Proceedings of the Ocean Drilling Program initial reports* (Vol. 145, pp. 209–302). Ocean Drilling Program.

Shipboard Scientific Party. (1995). Site 929. In W. B. Curry, & N. J. Shacklton (Eds.), *Proceedings of the Ocean Drilling Program initial reports* (Vol. 154, pp. 337–417). Ocean Drilling Program.

Shipboard Scientific Party. (1998). Site 1053. In R. D. Norris, & D. Kroon (Eds.), *Proceedings of the Ocean Drilling Program initial reports* (Vol. 171B, pp. 321–348). Ocean Drilling Program.

Shipboard Scientific Party. (1999a). Leg 177 Summary: Southern Ocean paleoceanography. In R. Gersonde, & D. A. Hodell (Eds.), *Proceedings of the Ocean Drilling Program initial reports* (Vol. 177, pp. 1–67). Ocean Drilling Program.

Shipboard Scientific Party. (1999b). Site 1090. In R. Gersonde, & D. A. Hodell (Eds.), *Proceedings of the Ocean Drilling Program initial reports* (Vol. 177, pp. 1–101). Ocean Drilling Program.

Shipboard Scientific Party. (2001a). Leg 189. In N. F. Exon, & J. P. Kennett (Eds.), *Proceedings of the Ocean Drilling Program initial reports* (Vol. 189, pp. 1–97). Ocean Drilling Program.

Shipboard Scientific Party. (2001b). Site 1170. In N. F. Exon, & J. P. Kennett (Eds.), *Proceedings of the Ocean Drilling Program initial reports* (Vol. 189, pp. 1–167). Ocean Drilling Program.

Shipboard Scientific Party. (2001c). Site 1171. In N. F. Exon, & J. P. Kennett (Eds.), *Proceedings of the Ocean Drilling Program initial reports* (Vol. 189, pp. 1–176). Ocean Drilling Program.

Shipboard Scientific Party. (2001d). Site 1172. In N. F. Exon, & J. P. Kennett (Eds.), *Proceedings of the Ocean Drilling Program initial reports* (Vol. 189, pp. 1–149). Ocean Drilling Program.

Shipboard Scientific Party. (2002). Site 1218. In M. Lyle, & P. A. Wilson (Eds.), *Proceedings of the Ocean Drilling Program initial reports* (Vol. 199, pp. 1–126). Ocean Drilling Program.

Shipboard Scientific Party. (2004a). Leg 208 summary. In J. C. Zachos, & D. Kroon (Eds.), *Proceedings of the Ocean Drilling Program initial reports* (Vol. 208, pp. 1–112). Ocean Drilling Program.

Shipboard Scientific Party. (2004b). Site 1263. In J. C. Zachos, & D. Kroon (Eds.), *Proceedings of the Ocean Drilling Program initial reports* (Vol. 208, pp. 1–87). Ocean Drilling Program.

Shipboard Scientific Party. (2004c). Site 1262. In J. C. Zachos, & D. Kroon (Eds.), *Proceedings of the Ocean Drilling Program initial reports* (Vol. 208, pp. 1–92). Ocean Drilling Program.

Shipboard Scientific Party. (2004d). Site 1266. In J. C. Zachos, D. Kroon, et al. (Eds.), *Proceedings of the Ocean Drilling Program initial reports* (Vol. 208, pp. 1–79). Ocean Drilling Program.

Shipboard Scientific Party. (2004e). Site 1267. In J. C. Zachos, & D. Kroon (Eds.), *Proceedings of the Ocean Drilling Program initial reports* (Vol. 208, pp. 1–77). Ocean Drilling Program.

Si, W., & Rosenthal, Y. (2019). Reduced continental weathering and marine calcification linked to late Neogene decline in atmospheric CO_2. *Nature Geoscience*, *12*, 833–838. https://doi.org/10.1038/s41561-019-0450-3

Siesser, W. G. (1995). Paleoproductivity of the Indian Ocean during the Tertiary Period. *Global and Planetary Change*, *11*, 71–88. https://doi.org/10.1016/0921-8181(95)00003-A

Sosdian, S. M., Rosenthal, Y., & Toggweiler, J. R. (2018). Deep Atlantic carbonate ion and $CaCO_3$ compensation during the Ice Ages. *Paleoceanography and Paleoclimatology*, *33*(6), 546–562. https://doi.org/10.1029/2017pa003312

Stickley, C. E., Brinkhuis, H., Schellenberg, S. A., Sluijs, A., Röhl, U., Fuller, M., et al. (2004). Timing and nature of the deepening of the Tasmanian gateway. *Paleoceanography*, *19*(4), PA4027. https://doi.org/10.1029/2004pa001022

Thomas, D. J. (2004). Evidence for deep-water production in the North Pacific Ocean during the early Cenozoic warm interval. *Nature*, *430*(6995), 65–67. https://doi.org/10.1038/nature02639

Thomas, D. J., Korty, R., Huber, M., Schubert, J. A., & Haines, B. (2014). Nd isotopic structure of the Pacific Ocean 70–30 Ma and numerical evidence for vigorous ocean circulation and ocean heat transport in a greenhouse world. *Paleoceanography*, *29*, 454–469. https://doi.org/10.1002/2013PA002535

Thomas, D. J., Lyle, M., Moore, T. C. Jr., & Rea, D. K. (2008). Paleogene deepwater mass composition of the tropical Pacific and implications for thermohaline circulation in a greenhouse world. *Geochemistry, Geophysics, Geosystems*, *9*(2), Q02002. https://doi.org/10.1029/2007GC001748

Thomas, E. (2007). Cenozoic mass extinctions in the deep sea: What disturbs the largest habitat on Earth? In S. Monechi, R. Coccioni, & M. Rampino (Eds.), *Large ecosystem perturbations: Causes and consequences* (pp. 1–24). Geological Society of America. https://doi.org/10.1130/2007.2424(01)

Thunell, R., & Corliss, B. H. (1986). Late Eocene-early Oligocene carbonate sedimentation in the deep sea. In C. Pomero, & I. Premoli-Silva (Eds.), *Terminal Eocene events* (pp. 363–380). Elsevier. https://doi.org/10.1016/s0920-5446(08)70140-7

Tripati, A., Backman, J., Elderfield, H., & Ferretti, P. (2005). Eocene bipolar glaciation associated with global carbon cycle changes. *Nature*, *436*(7064), 341–346. https://doi.org/10.1038/nature04289

Tripati, A., & Darby, D. (2018). Evidence for ephemeral middle Eocene to early Oligocene Greenland glacial ice and pan-Arctic sea ice. *Nature Communications*, *9*(1), 1038. https://doi.org/10.1038/s41467-018-03180-5

Vahlenkamp, M., Niezgodzki, I., De Vleeschouwer, D., Lohmann, G., Bickert, T., & Pälike, H. (2018). Ocean and climate response to North Atlantic seaway changes at the onset of long-term Eocene cooling. *Earth and Planetary Science Letters*, *498*, 185–195. https://doi.org/10.1016/j.epsl.2018.06.031

Van Andel, T. H. (1975). Mesozoic/Cenozoic calcite compensation depth and the global distribution of calcareous sediments. *Earth and Planetary Science Letters*, *26*(2), 187–194. https://doi.org/10.1016/0012-821x(75)90086-2

Via, R. K., & Thomas, D. J. (2006). Evolution of Atlantic thermohaline circulation: Early Oligocene onset of deep water production in the North Atlantic. *Geology*, *34*(6), 441–444. https://doi.org/10.1130/g22545.1

Wade, B. S., Houben, A. J. P., Quaijtaal, W., Schouten, S., Rosenthal, Y., Miller, K. G., et al. (2012). Multiproxy record of abrupt sea-surface cooling, across the Eocene-Oligocene transition in the Gulf of Mexico. *Geology*, *40*(2), 159–162. https://doi.org/10.1130/g32577.1

Wade, B. S., & Pearson, P. N. (2008). Planktonic foraminiferal turnover, diversity fluctuations and geochemical signals across the Eocene/Oligocene boundary in Tanzania. *Marine Micropaleontology*, *68*(3–4), 244–255. https://doi.org/10.1016/j.marmicro.2008.04.002

Wagner, T. (2002). Late Cretaceous to early Quaternary organic sedimentation in the eastern equatorial Atlantic. *Palaeogeography, Palaeoclimatology, Palaeoecology*, *179*(1–2), 113–147. https://doi.org/10.1016/S0031-0182(01)00415-1

Walker, J. C. G., Hays, P. B., & Kasting, J. F. (1981). A negative feedback mechanism for the long-term stabilization of Earth's surface temperature. *Journal of Geophysical Research: Oceans*, *86*(C10), 9776–9782. https://doi.org/10.1029/JC086iC10p09776

Westerhold, T., Marwan, N., Drury, A. J., Liebrand, D., Agnini, C., Anagnostou, A., et al. (2020). An astronomically dated record of Earth's climate and its predictability over the last 66 million years. *Science*, *369*, 1383–1387. https://doi.org/10.1126/science.aba6853

Westerhold, T., Röhl, U., Pälike, H., Wilkens, R., Wilson, P. A., & Acton, G. (2014). Orbitally tuned timescale and astronomical forcing in the middle Eocene to early Oligocene. *Climate of the Past*, *10*, 955–973. https://doi.org/10.5194/cp-10-955-2014

Westerhold, T., Röhl, U., Wilkens, R., Pälike, H., Lyle, M., Jones, T. D., et al. (2012). Revised composite depth scales and integration of IODP Sites U1331-U1334 and ODP Sites 1218-1220. In H. Pälike, M. Lyle, H. Nishi, I. Raffi, K. Gamage, A. Klaus (Eds.), & the Expedition 320/321 Scientists. (Eds.), *Proceedings of the international ocean discovery Program* (Vol. 320/321, pp. 1–137). Integrated Ocean Drilling Program.

Zachos, J., Pagani, M., Sloan, L., Thomas, E., & Billups, K. (2001). Trends, rhythms and aberration in global climate 65 Ma to present. *Science*, *292*(5517), 686–693. https://doi.org/10.1126/science.1059412

Zachos, J., Stott, L. D., & Lohmann, K. C. (1994). Evolution of the early Cenozoic marine temperatures. *Paleoceanography*, *9*(2), 3153–3387. https://doi.org/10.1029/93PA03266

Zachos, J. C., Opdyke, B. N., Quinn, T. M., Jones, C. E., & Halliday, A. N. (1999). Early Cenozoic glaciation, Antarctic weathering, and seawater [87]Sr/[86]Sr: Is there a link? *Chemical Geology*, *161*(1-3), 165–180. https://doi.org/10.1016/S0009-2541(99)00085-6

Zachos, J. C., Rea, D. K., Seto, K., Nomura, R., & Nitsuma, N. (1992). Paleogene and early Neogene deep water paleoceanography of the Indian Ocean as determined from benthic foraminifer stable carbon and oxygen isotope records. In R. A. Duncan, D. K. Rea, R. B. Kidd, U. von Rad, & J. K. Weissel (Eds.), *Synthesis of results from scientific drilling in the Indian Ocean* (Vol. 70, pp. 351–386). American Geophysical Union.

Zeebe, R. E. (2012). History of seawater carbonate chemistry, atmospheric CO_2, and ocean acidification. *Annual Review of Earth and Planetary Sciences*, *40*, 141–165. https://doi.org/10.1146/annurev-earth-042711-105521

Zeebe, R. E., & Wolf-Gladrow, D. (2001). CO_2 *in seawater: Equilibrium, kinetics, isotopes*. Elsevier.

References From the Supporting Information

Berggren, W., Kent, D., Swisher, C., III, & Aubry, M.-P. (1995). A revised Cenozoic geochronology and chronostratigraphy. In W. Berggren, D. V. Kent, M.-P. Aubry, & J. Hardenbol (Eds.), *Geochronology, time scales and global stratigraphic correlation, SEPM special publication* (Vol. 54, pp. 129–212). Society for Sedimentary Geology. https://doi.org/10.2110/pec.95.04.0129

Berggren, W. A., Kent, D. V., & Flynn, J. J. (1985). Jurassic to Paleogene: Part 2. Paleogene geochronology and chronostratigraphy. In N. J. Snelling (Ed.), *The chronology of the geologic record. The geological society memoir* (Vol. 10, pp. 141–195). The Geological Society. https://doi.org/10.1144/gsl.mem.1985.010.01.15

Cande, S. C., & Kent, K. D. (1995). Revised calibration of the geomagnetic polarity timescale for the Late Cretaceous and Cenozoic. *Journal of Geophysical Research: Solid Earth*, *111*, 6093–6095. https://doi.org/10.1029/94JB03098

Gradstein, F. M., Ogg, J. G., & Smith, A. G. (2005). *A geological time scale 2004*. Cambridge University Press.